Advected fields in maps: III. Passive scalar decay in baker's maps

Andrew D. Gilbert

Department of Mathematical Sciences, University of Exeter, EX4 4QE, U.K.

Abstract

The decay of passive scalars is studied in baker's maps with uneven stretching, in the limit of weak diffusion. The map is alternated with diffusion, and three different boundary conditions are employed, zero boundaries, no-flux boundaries, and periodic boundaries. Numerical results are given for scalar decay modes.

A set of eigenmode branches and eigenfunctions is also set up for case of zero diffusion, using a complex variable formulation. The effects of diffusion may then be included by means of a boundary layer theory. Depending on the boundary conditions, the effect of diffusion is to either simply perturb or entirely destroy each zero-diffusion branch.

The paper considers analytically the decay of passive scalar fluctuations for each boundary condition, and elucidates scaling laws that govern the behaviour of eigenvalues in the limit of weak diffusion.

Key words: Passive scalar, hyperbolic map, mixing, baker's map, diffusion, Ruelle–Pollicott resonance.

1 Introduction

This paper concerns the mixing and decay of passive scalars under the action of baker's maps. These idealised models are prototypes for understanding the mixing and decay of scalar fluctuations in fluid flows. Here the mathematical challenge arises because the interaction of the stretching and folding of scalar concentration, with weak molecular diffusion, gives complex scalar fields which are hard to describe and analyse. Key references include [2] and [26].

One way to simplify the problem is to replace a fluid flow by a Lagrangian mapping and to consider models where one alternatively applies the mapping, say M, instantaneously and then allows diffusion of strength ε to operate for a unit time. The advantage is that one can write down explicitly how a scalar

field, say $a(\boldsymbol{x})$, is mapped to a new scalar field, say $T_\varepsilon a$, after one iteration of the map–diffuse cycle. The mathematical problem remains challenging though, because for small ε the field can adopt complicated structures under repeated application of T_ε, especially in the case where the mapping M possesses chaotic trajectories.

One attractive family of maps to study is that of baker's maps, as the scalar fields can be taken to be one-dimensional, and the mappings are hyperbolic. These have been used a great deal in modelling the behaviour of passive scalars, and the closely analogous phenomenon of magnetic field amplification in conducting fluid flows, the kinematic dynamo. For example Ott and Antonsen [25] consider advection of scalar and vector fields and show that the scalar gradient and vector field concentrate on fractal sets under iterations of T_ε with weak diffusion. The problem of how passive scalars decay in baker's maps has been discussed in [13,14,37]. For magnetic fields dynamo action in baker's maps has been studied by Finn and Ott [15,16] and in the closely related stretch–fold–shear model by Bayly and Childress [7,8]; for a review see [10].

While baker's maps have been widely studied as a prototype dynamical system, including the complications of uneven stretching and folding, little is known mathematically about the effects of weak diffusion of passive scalar or of magnetic field in even these very simplified systems. Our aim in this paper and two earlier studies [18,19] is to understand the effects of diffusion. We use a combination of boundary layer theory, and complex variable methods that allow us to make sense of a problem with zero diffusion and define what are known as 'strange eigenfunctions' [23,27,34]. These are 'eigenfunctions' that take the form of distributions rather than well-behaved functions. They have been discussed in the kinematic dynamo problem [6,10], though not under this name, and observed experimentally as limiting scalar field structures for weak diffusion [31].

Our aim is to explain the observations of passive scalar decay in baker's maps discussed in [14,37]. For example these authors note that the decay of passive scalars with periodic boundary conditions is oscillatory, corresponding to a complex eigenvalue λ of the operator T_ε, and that the approach to the diffusionless limit is very slow, only logarithmic with diffusion ε. Also in an idealised Gaussian model [37] a decay rate is found that is sensitive to the boundary conditions employed during the diffusion step. We find this to be true in our study also, and this feature has been noticed in analogous dynamo problems [16].

The paper is structured as follows. Section 2 introduces the baker's map and presents results for scalar decay under various boundary conditions, showing the sensitivity noted by previous authors. Eigenfunctions and adjoint eigen-

functions are also plotted, and it is seen that whereas the direct eigenfunctions (that is of T_ε) have fine structure for small ε, adjoint eigenfunctions (that is of T_ε^*) are smooth, except for boundary layers at the edges of the region mapped.

Section 3 studies the decay of a scalar with the zero boundary condition. This corresponds to allowing scalar to leak out of the domain when it diffuses, and we find the leakage rate, i.e., the exponential decay rate of scalar, approximately for small ε, by using a boundary layer theory and a solvability condition. In section 4 we set up a complex variable framework which enables us to define eigenvalues $\lambda_{(n)}$ for zero diffusion. The corresponding adjoint eigenfunctions (that is of T^*) are polynomials, but those of T can only be thought of as distributions; these are 'strange eigenfunctions'. Section 5 uses these strange eigenfunctions to discover which $\lambda_{(n)}$ survive the introduction of diffusion. It also enables us to give approximate formulae for the decay rate of scalar fluctuations in the baker's map under a no-flux boundary condition.

Section 6 discusses the decay of passive scalar fluctuations with a periodic boundary condition and shows why the corresponding eigenvalues governing decay of scalar fluctuations are complex and converge logarithmically slowly in the limit of weak diffusion. Section 7 discusses a baker's map involving a fold operation which has some unusual features. In particular for the no-flux boundary condition the eigenvalue governing decay of scalar fluctuations has an oscillatory behaviour as a function of the diffusivity ε as $\varepsilon \to 0$. This surprising feature has been noted in a related model [13].

Our study will link closely to ideas in dynamical systems theory: for example the eigenvalues $\lambda_{(n)}$ that we obtain for passive scalar decay for zero diffusion are actually what are known as Ruelle–Pollicott resonances [29,32]. We will revisit this in the final discussion section 8.

2 Numerical results with diffusion

We are interested in the evolution of passive scalars in baker's maps, with weak diffusion. The baker's map we will use is depicted schematically in figure 1 and is given by a parameter α with $0 < \alpha < 1$. We also define

$$\beta \equiv 1 - \alpha, \quad \Upsilon \equiv -1 + 2\alpha \equiv 1 - 2\beta \equiv \alpha - \beta. \tag{2.1}$$

It is convenient to define the baker's map on the square $-1 \le x, y \le 1$ by

$$M(x,y) = \begin{cases} (\alpha x - \beta, \alpha^{-1}(y+\beta)) & (-1 \le y \le \Upsilon), \\ (\beta x + \alpha, \beta^{-1}(y-\alpha)) & (\Upsilon < y \le 1). \end{cases} \tag{2.2}$$

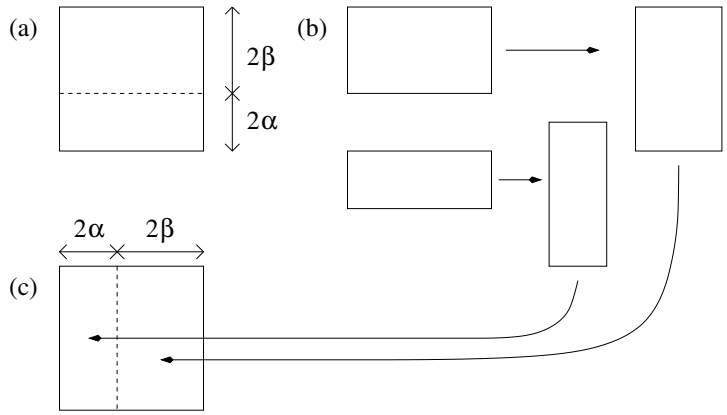

Fig. 1. The uneven baker's map. (a) The square $[-1,1]^2$ is cut horizontally. (b) The two pieces are stretched and (c) reassembled.

The map is symmetrical under the interchange of α and β and reversal of the x-direction.

We consider the evolution of a passive scalar field $a(x)$, which we will occasionally refer to as temperature: under one iteration of the map M, the temperature field is mapped to

$$Ta(x) = \begin{cases} a(\alpha^{-1}(x+\beta)) & (-1 \le x \le \Upsilon), \\ a(\beta^{-1}(x-\alpha)) & (\Upsilon < x \le 1). \end{cases} \tag{2.3}$$

Note that to avoid unnecessary use of brackets we write $Ta(x)$ rather than the more pedantic version $(Ta)(x)$ here and elsewhere.

We will make considerable use of the adjoint operator T^*. To define this we start with an inner product on $L^2[-1,1]$:

$$(b,a) = \int_{-1}^{1} b(x)a(x)\,dx. \tag{2.4}$$

This may also be thought of as the action of a member b of the dual space (again $L^2[-1,1]$) on a function a, which is why we do not place a complex conjugate in this definition. The L^2 norm (for functions on $[-1,1]$ henceforth understood) is given by

$$\|a\|^2 = (\overline{a}, a) \qquad (\overline{a}(x) \equiv \overline{a(x)}). \tag{2.5}$$

The adjoint operator T^* is then defined by $(b, Ta) = (T^*b, a)$ and is given by

$$T^*b(x) = \alpha b(\alpha x - \beta) + \beta b(\beta x + \alpha). \tag{2.6}$$

A trivial but important eigenvalue of T and T^* is $\lambda = 1$, with a constant field in each case. We have $Ta = \lambda a$ and $T^*b = \lambda b$ and label it with zero subscript

as

$$a_{(0)} = \tfrac{1}{2}, \quad b_{(0)} = 1, \quad \lambda_{(0)} = 1 \quad \text{(constant scalar mode)}. \tag{2.7}$$

This is conveniently normalised so that

$$(a_{(0)}, b_{(0)}) = 1. \tag{2.8}$$

We now wish to consider the evolution of a passive scalar under T and weak diffusion, and so after each application of T, we apply diffusion, solving $\partial_t a = \varepsilon \nabla^2 a$ for a time unity in the region $-1 \le x \le 1$ with suitable boundary conditions. One aim of this paper is to understand the effect of boundary conditions, and so we consider zero temperature (Z), no-flux or insulating (F), and periodic (P) boundary conditions, defined by

$$a(\pm 1) = 0 \qquad \text{(Z)}, \tag{2.9}$$

$$\partial_x a(\pm 1) = 0 \qquad \text{(F)}, \tag{2.10}$$

$$a(x) \text{ periodic} \qquad \text{(P)}. \tag{2.11}$$

We will also occasionally find the asymmetric zero–no-flux boundary condition (ZF) useful, though we will not treat it as thoroughly as the other cases. This is defined by

$$a(-1) = 0, \quad \partial_x a(1) = 0 \qquad \text{(ZF)}, \tag{2.12}$$

and breaks the symmetry of interchanging α and β.

Diffusion can be achieved by integrating the scalar field against a heat kernel $H_\varepsilon(x, y)$ incorporating the appropriate boundary condition. We use the symbol H_ε also for the resulting operator, given by

$$H_\varepsilon a(x) = \int_{-1}^{1} H_\varepsilon(x, y) a(y)\, dy. \tag{2.13}$$

We have for zero (upper sign) and no-flux (lower sign) boundary conditions,

$$H_\varepsilon(x, y) = \sum_{p \text{ even}} G_\varepsilon(x - y - 2p) \mp \sum_{p \text{ odd}} G_\varepsilon(x + y - 2p) \quad \text{(Z/F)}, \tag{2.14}$$

and for the periodic boundary condition

$$H_\varepsilon(x, y) = \sum_{p} G_\varepsilon(x - y - 2p) \quad \text{(P)}. \tag{2.15}$$

In each case p ranges over the integers, and

$$G_\varepsilon(x) = \varepsilon^{-1/2} g(x/\sqrt{\varepsilon}), \qquad g(x) = (4\pi)^{-1/2} \exp(-x^2/4). \tag{2.16}$$

We then define the scalar transport operator with diffusion, T_ε, and its adjoint T_ε^* by

$$T_\varepsilon = H_\varepsilon T, \qquad T_\varepsilon^* = T^* H_\varepsilon^*, \tag{2.17}$$

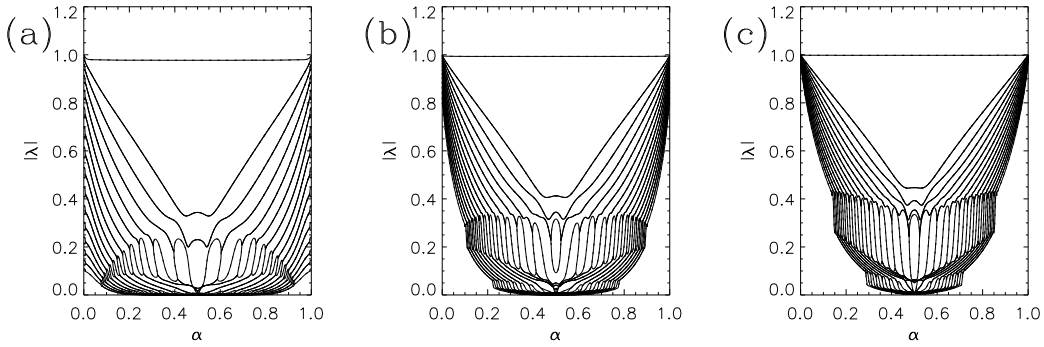

Fig. 2. Moduli of eigenvalues $|\lambda|$ as a function of α for the zero boundary condition (Z). The values for the diffusivity and resolution are (a) $\varepsilon = 10^{-3}$, $N = 128$, (b) $\varepsilon = 10^{-4}$, $N = 512$ and (c) $\varepsilon = 10^{-5}$, $N = 1024$.

noting that H_ε is self-adjoint, $H_\varepsilon^* = H_\varepsilon$. For positive ϵ both of these operators are compact in L^2 and so have spectra consisting of only point spectrum, i.e., discrete eigenvalues. For each eigenvalue λ, there will be a pair of eigenfunctions, of T_ε and T_ε^*,

$$T_\varepsilon a = \lambda a, \quad T_\varepsilon^* b = \lambda b. \tag{2.18}$$

Corresponding to any given eigenvalue λ there will be an exponential growth rate $p = \log \lambda$, with negative (or zero) real part; for example, the asymptotic scalar variance decays proportional to e^{2np} as the number of iterations $n \to \infty$.

To obtain eigenvalues λ numerically it makes sense to use a real orthonormal basis $\{\psi_n\}$ of L^2 adapted to the boundary conditions, and to compute matrix elements

$$T_{mn} = (\psi_m, T\psi_n), \quad H_{\varepsilon mn} = (\psi_m, H_\varepsilon \psi_n). \tag{2.19}$$

The matrices may then be truncated to size N^2 and eigenvalues found numerically. The corresponding right and left eigenvectors of $T_{\varepsilon mn}$ give the direct and adjoint eigenfunctions a and b in (2.18) above. The bases and matrix elements are given in appendix A.

We now present results, plotting the moduli $|\lambda|$ of the eigenvalues λ of T_ε against α for given values of ε. In each case we show only the leading 30 branches, and the resolution in α in the plots is 0.001. Figure 2 shows results for the case of the zero boundary condition, with $\varepsilon = 10^{-3}$ in (a), 10^{-4} in (b) and 10^{-5} in (c). The resolutions N are given in the caption, and in each case the curves are overplotted with results at a resolution $N/2$ in dotted lines. These cannot be seen, and this confirms the accuracy of the results shown; dotted lines are used similarly in figures 4, 6, 8 and 22 below.

In each of figure 2(a,b,c) we see clearly the branch corresponding to the constant scalar mode (2.7); however this is now perturbed because of diffusion under the zero boundary condition. Scalar escapes from the system and this

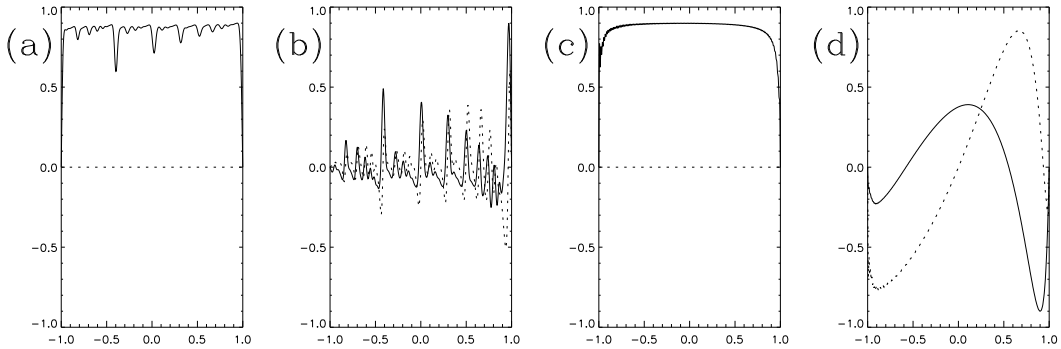

Fig. 3. Eigenfunctions for $\alpha = 0.3$, $\varepsilon = 10^{-4}$ and the zero (Z) boundary condition. Solid lines show the real part and dotted the imaginary part. (a) depicts the least damped and (b) the next least damped eigenmode of T_ε. (c) and (d) show the corresponding eigenmodes for T_ε^*.

mode now decays. In fact we will find that for this mode

$$\lambda \simeq 1 + [C_0(\alpha) + C_0(\beta)]\varepsilon^{1/2}, \tag{2.20}$$

where we shall obtain the (negative) constants C_0 by solving a boundary layer problem for each value of α, in section 3. The contributions $C_0(\alpha)$ and $C_0(\beta)$ arise because of loss of scalar through the left- and right-hand boundaries. The corresponding direct eigenfunction is shown in figure 3(a) for $\alpha = 0.3$ and $\varepsilon = 10^{-4}$, and can be seen to be the constant scalar mode, $a_{(0)}$ in (2.7), perturbed by accumulating internal boundary layers, which decrease in scale and increase in number as ε is reduced.

However the corresponding adjoint eigenfunction, shown in figure 3(c) has a much simpler structure, and is essentially the constant scalar mode, $b_{(0)}$ in (2.7), with a boundary layer at each end. As ε is reduced, the boundary layers become narrower, but the interior tends to a constant. This arises because the adjoint operator T^* in (2.6) tends to pull out and smooth fine structure, in contrast to T. This property is what allows possible analytical study of the awkward limit $\varepsilon \to 0$, and was originally stressed in related dynamo problems by Bayly and Childress [8].

Note that this leading mode as shown in figure 3(a,c) is the key mode governing scalar decay in the system; even if the mean scalar is taken to be zero in an initial condition, this will not generally be preserved by the zero boundary condition as T_ε is iterated. The lower branches in figure 2 are therefore perhaps only of theoretical interest; they seem to accumulate as diffusion is reduced. The next branch down in fact corresponds to a complex conjugate pair of eigenvalues. One of the pair of direct eigenfunctions is shown in figure 3(b), and the corresponding adjoint eigenfunction in figure 3(d); both are complex. Note again that the adjoint eigenfunction is much smoother than the direct one.

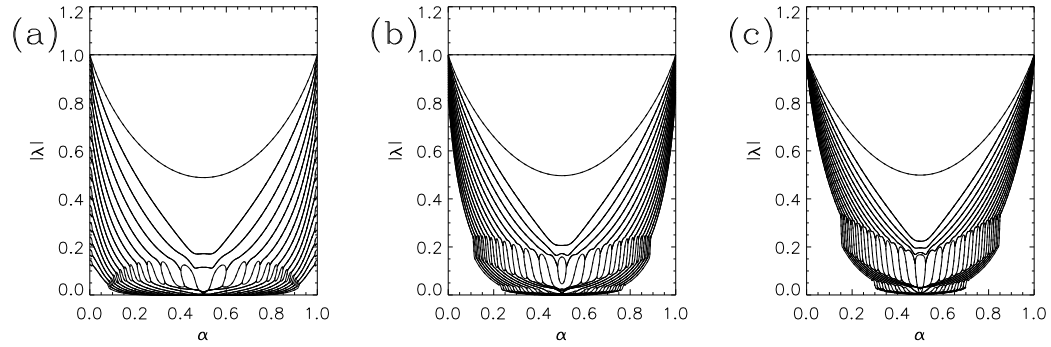

Fig. 4. As for figure 2 but with the no-flux (F) boundary condition.

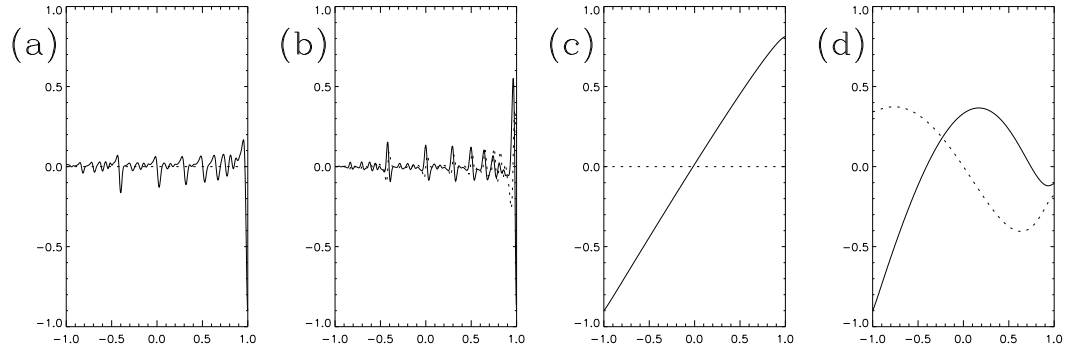

Fig. 5. Eigenfunctions as in figure 3 but for the no-flux (F) boundary condition, except that we exclude the constant mode (2.7).

Figure 4 shows results for the no-flux (F) boundary condition. Now the constant scalar mode (2.7) satisfies the boundary condition and so remains there as an exact $\lambda = 1$ branch. The next branch down is new, not present for the zero boundary condition in figure 2, and corresponds to a scalar field with zero mean. This branch therefore governs the decay of scalar fluctuations in the system, and is the key mode to study analytically. We will in fact find that for this mode there are contributions from the two boundaries, with

$$\lambda \simeq \lambda_{(1)} + C_1(\alpha,\varepsilon)\varepsilon^{q(\alpha)} + C_1(\beta,\varepsilon)\varepsilon^{q(\beta)}, \qquad \lambda_{(1)} = \alpha^2 + \beta^2, \tag{2.21}$$

where we will pin down the exponents q analytically (see (5.14)) and obtain the quantities C_1 (which vary only weakly with ε) by solving a boundary layer problem numerically, in section 5.

The direct and adjoint eigenfunctions for this mode (with $\alpha = 0.3$, $\varepsilon = 10^{-4}$) are shown in figure 5(a,c) respectively. Again while the direct eigenfunction is very irregular, the adjoint eigenfunction appears to be tending to a linear function, with boundary layers at each end, open to analysis. The next, third branch down in figure 4 corresponds to a complex conjugate pair of eigenvalues λ, and figure 5(b,d) shows one of the eigenfunction pairs.

To stress the role of boundary conditions figure 6 shows eigenvalues for the

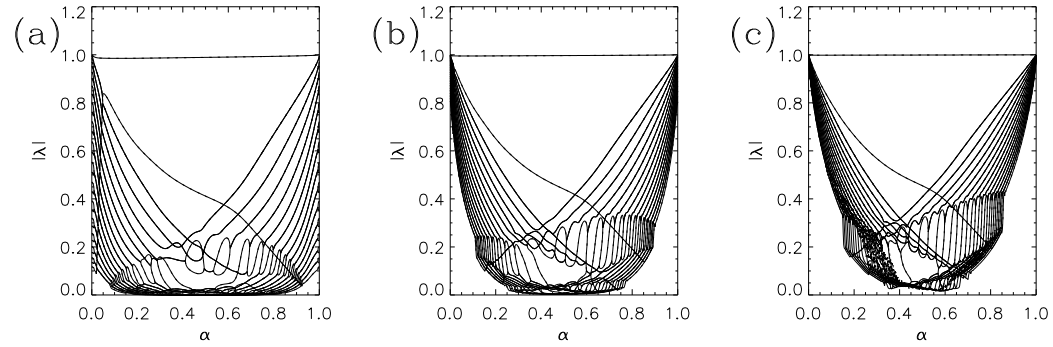

Fig. 6. As for figure 2 but with the zero–no-flux (ZF) boundary condition. Note that some numerical noise is apparent in (c) for the $N = 512$ resolution results, shown dotted.

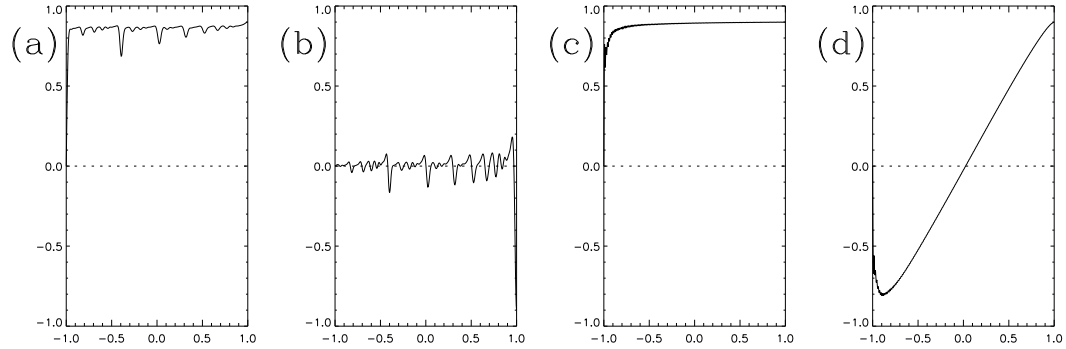

Fig. 7. Eigenfunctions as in figure 3 but for the zero–no-flux (ZF) boundary condition.

zero–no-flux boundary condition (2.12), and figure 7 the corresponding eigenfunctions for the leading two branches. The first branch is again linked to the constant scalar mode (2.7), now decaying because of the left-hand zero boundary condition (cf. figure 3(a,c)). Its decay rate is given by a formula

$$\lambda \simeq 1 + C_0(\alpha)\varepsilon^{1/2}, \tag{2.22}$$

akin to (2.20). On the other hand for $\alpha < \frac{1}{2}$, the second branch down in figure 6 has features in common with the second branch for the no-flux (F) boundary condition in figure 4. For this branch eigenfunctions for the (ZF) boundary condition are shown in figure 7(b,d) and for the (F) boundary condition in figure 5(a,c).

Finally figure 8 shows the case of the periodic boundary condition. The leading branch is the constant scalar solution (2.7), again exactly preserved by the boundary condition. The remaining branches seem to accumulate as the diffusivity is reduced, and correspond to pairs of complex conjugate eigenvalues. Figure 9 shows a complex eigenfunction for the first two non-trivial branches. In section 6 we will establish that for $\alpha \neq \beta$

$$\lambda = \max(\alpha, \beta) + o(\varepsilon) \tag{2.23}$$

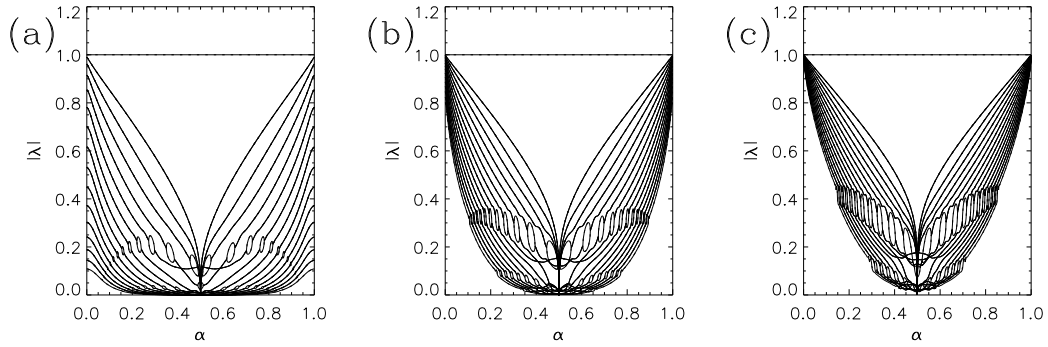

Fig. 8. As for figure 2 but with the periodic (P) boundary condition.

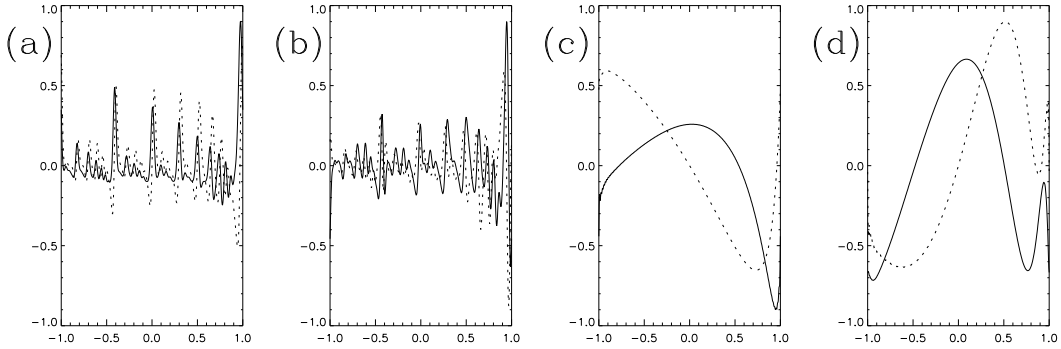

Fig. 9. Eigenfunctions as in figure 3 but for the periodic (P) boundary condition, except that we exclude the constant mode (2.7).

as $\varepsilon \to 0$, where the leading correction in $o(\varepsilon)$ is purely imaginary and decreases as the inverse of $\log \varepsilon^{-1}$.

For $\alpha = \beta = \frac{1}{2}$ all branches, except the constant-scalar one, go to zero with the periodic boundary condition. In this case the action of T_ε on the appropriate basis (A.3) is given by

$$T_\varepsilon \cos q\pi x = e^{-4\varepsilon q^2\pi^2}(-1)^q \cos 2q\pi x, \qquad T_\varepsilon \sin q\pi x = e^{-4\varepsilon q^2\pi^2}(-1)^q \sin 2q\pi x. \tag{2.24}$$

From this it is easily deduced that there are no eigenfunctions of T_ε in L^2 except the constant scalar one (2.7), and that zero-mean fields undergo super-exponential decay [14]. Note that by similar arguments, for the (Z) boundary condition there is super-exponential decay for the subspace of odd fields (n even in (A.1)), and for (F) this occurs for even non-constant fields ($n > 0$ and even in (A.2)).

To summarise, we are primarily interested in the first non-trivial decay mode in each case: this means

(i) (Z) boundary condition, first branch of figure 2, eigenfunctions in figure 3(a,c), and formula (2.20); see section 3,
(ii) (F) boundary condition, second branch of figure 4, eigenfunctions in figure

5(a,c), and formula (2.21); see section 5,

(iii) (P) boundary condition, second branch of figure 8, eigenfunctions in figure 9(a,c); see section 6.

3 Scalar decay with the zero boundary condition

Since it requires no special machinery, we begin our analysis by studying the decay of scalar in the case of the zero boundary condition. In other words we wish to understand how the constant scalar mode (2.7) is modified by diffusion to give decay according to (2.20). We give a fairly detailed exposition, as it will be the basis for later calculations in sections 5, 6, where we will be more succint.

We home in on the adjoint eigenfunction shown in figure 3(c) which clearly has the structure of a constant 'mainstream' interior with boundary layers at each end, $x = \pm 1$. We write

$$T^*_\varepsilon = T^* + T^*_1, \qquad T^*_1 \equiv T^*(H_\varepsilon - I), \tag{3.1}$$

thinking of T^*_1 as a small perturbation to T^*, and aim to solve

$$T^*_\varepsilon b = (T^* + T^*_1)b = \lambda b \qquad (0 < \varepsilon \ll 1) \tag{3.2}$$

approximately. We expand λ, a (the adjoint eigenfunction) and b by

$$\lambda = \lambda_0 + \lambda_1 + \cdots, \quad a = a_0 + a_1 + \cdots, \quad b = b_0 + b_1 + \cdots, \tag{3.3}$$

where $\lambda_0 = \lambda_{(0)}$, and $a_0 = a_{(0)}$, $b_0 = b_{(0)}$ is the constant scalar mode defined in (2.7) and normalised by (2.8). $\lambda_1 \ll 1$ is the leading correction to the eigenvalue, and b_1 the leading correction to the eigenfunction (2.7) generated by the perturbation T^*_1.

Substituting into (3.2), subtracting off $T^* b_0 = \lambda_0 b_0$ and retaining all possible leading terms gives an equation for b_1 forced by the term $T^*_1 b_0$,

$$T^*_1 b_0 + T^*_\varepsilon b_1 = \lambda_0 b_1 + \lambda_1 b_0. \tag{3.4}$$

This equation describes both the boundary layer structure and the mainstream correction, though different elements come into dominance in different regions. We define the mainstream region by

$$-1 < x < 1, \qquad x \text{ fixed as } \varepsilon \to 0, \tag{3.5}$$

and the two boundary layers by

$$x \equiv -1 + \sqrt{\varepsilon} X \quad \text{(left)}, \quad x \equiv 1 - \sqrt{\varepsilon} X \quad \text{(right)}, \quad X \text{ fixed as } \varepsilon \to 0. \tag{3.6}$$

We take b_1 to vary on the X-scale in the boundary layers, and on the longer, x-scale in the mainstream. The key feature of the mainstream is that diffusion can be ignored at leading order, since for functions here varying on the x-scale,

$$H_\varepsilon = I + O(\varepsilon). \tag{3.7}$$

Let us focus on the left-hand boundary layer with $X = O(1)$, $x \simeq -1$ and consider each term of (3.4) in turn. In the layer, we may approximate $H_\varepsilon(x, y)$ from (2.14) by retaining only the terms $p = 0, -1$. We then compute, using (2.7) and (2.16),

$$(H_\varepsilon - I)b_0(-1 + \sqrt{\varepsilon}X) \simeq -2g_0(X), \tag{3.8}$$

where we define, for future use,

$$g_n(s) = \int_0^\infty g(s + t)t^n \, dt \tag{3.9}$$

with

$$g_0(s) = \tfrac{1}{2}\operatorname{erfc}(s/2). \tag{3.10}$$

This yields the first term in (3.4) as

$$T_1^* b_0(-1 + \sqrt{\varepsilon}X) = -2\alpha g_0(\alpha X), \tag{3.11}$$

a source term that is localised on the X-scale, vanishing rapidly as $X \to \infty$, and which drives the boundary layer.

The second term in (3.4) in the boundary layer is

$$T_\varepsilon^* b_1(-1 + \sqrt{\varepsilon}X) \simeq \alpha H_\varepsilon b_1(-1 + \sqrt{\varepsilon}\alpha X) + \beta b_1(\Upsilon). \tag{3.12}$$

Here through the action of T_ε^* we have picked up a contribution from $x \simeq \Upsilon$ in the mainstream and we have also neglected diffusion there using (3.7). In the boundary layer H_ε can again be approximated by retaining terms $p = 0, -1$ in (2.14).

We have so far made no assumptions about the magnitude of b_1 and λ_1. However below we shall find that $b_1 = O(1)$ in the boundary layer, being forced by the term (3.11), but decays to take values of size $b_1 = O(\sqrt{\varepsilon})$ in the mainstream (see (3.16)). Also we shall find below that $\lambda_1 = O(\sqrt{\varepsilon})$ (see (3.22)). This means that in the boundary layer we can neglect $\lambda_1 b_0$ in (3.4) and $\beta b_1(\Upsilon)$ in (3.12), and then (3.4) becomes the integral equation

$$-2\alpha g_0(\alpha X) + \alpha \int_0^\infty [g(\alpha X - Y) - g(\alpha X + Y)]d(Y) \, dY = \lambda_0 d(X), \tag{3.13}$$

where we set

$$b_1(-1 + \sqrt{\varepsilon}X) = d(X). \tag{3.14}$$

Now to link this to the mainstream solution we need the far field $X \to \infty$. Here the source term (3.11) goes rapidly to zero, diffusion drops out and we are left with

$$\alpha \int_0^\infty g(\alpha X - Y) d(Y)\, dY \simeq \alpha d(\alpha X) = \lambda_0 d(X) \tag{3.15}$$

as an approximation to (3.4) valid in an overlap region $1 \ll X \ll \varepsilon^{-1/2}$ between boundary layer and mainstream (see (3.17)). The solution is

$$d(X) = X^{-1} f(\log X), \qquad (f \text{ periodic, period } \log \alpha), \tag{3.16}$$

with $\lambda_0 = 1$ substituted. For the right-hand boundary layer the theory goes through identically with α replaced by β.

We now consider the solution in the mainstream, defined in (3.5), for which (3.4) reduces at leading order to

$$T^* b_1 = \lambda_0 b_1 + \lambda_1 b_0. \tag{3.17}$$

Here we have used (3.7) to replace T_ε^* with T^*. The form of (3.17) suggests employing a solvability condition, multiplying by the adjoint eigenfunction a_0 and integrating; however we cannot integrate all the way from -1 to 1, and have to exclude boundary layers. Let μ be a parameter satisfying $\sqrt{\varepsilon} \ll \mu \ll 1$ and consider

$$\int_{-1+\mu}^{1-\mu} a_0 (T^* - \lambda_0) b_1 \, dx = \lambda_1 \int_{-1+\mu}^{1-\mu} a_0 b_0 \, dx \simeq \lambda_1 (a_0, b_0) = \lambda_1, \tag{3.18}$$

using (2.8). However using the form of T^* in (2.6), we have

$$\int_{-1+\mu}^{1-\mu} a_0 T^* b_1 \, dx = \left(\int_{-1+\alpha\mu}^{\Upsilon - \alpha\mu} + \int_{\Upsilon+\beta\mu}^{1-\beta\mu} \right) (T a_0) b_1 \, dx. \tag{3.19}$$

With $T a_0 = \lambda_0 a_0$ and substituting into (3.18) we obtain

$$\lambda_1 = \lambda_0 \left[\int_{-1+\alpha\mu}^{-1+\mu} + \int_{1-\mu}^{1-\beta\mu} - \int_{\Upsilon-\alpha\mu}^{\Upsilon+\beta\mu} \right] a_0 b_1 \, dx. \tag{3.20}$$

Of course here $a_0 = 1/2$ and $\lambda_0 = 1$ so we just have integrals of b_1 over short segments to deal with. Given that b_1 increases to $O(1)$ as we approach the boundary layers, but is only $O(\sqrt{\varepsilon})$ in the mainstream, the third integral may be neglected. The contribution from the left-hand boundary layer arises from the first integral, which amounts to

$$\lambda_{1\mathrm{L}} \equiv \tfrac{1}{2} \int_{-1+\alpha\mu}^{-1+\mu} b_1 \, dx = \tfrac{1}{2} \sqrt{\varepsilon} \int_{\alpha Y}^{Y} d(X) \, dX \tag{3.21}$$

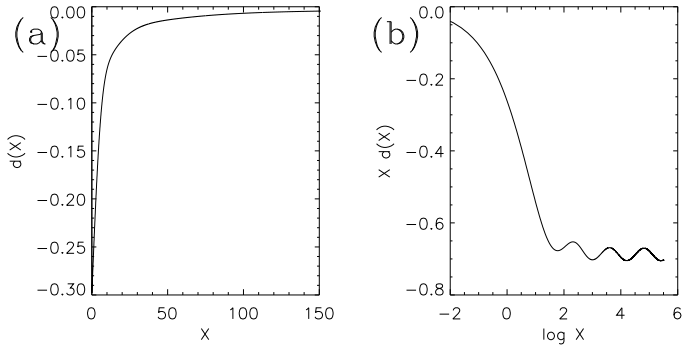

Fig. 10. Solution to boundary layer integral equation (3.13), showing (a) $d(X)$ against X, and (b) $Xd(X)$ against $\log X$.

with $Y = \mu/\sqrt{\varepsilon} \gg 1$ and using (3.14). So finally we obtain the eigenvalue correction, including the right-hand boundary layer, as

$$\lambda_1 = (C_0(\alpha) + C_0(\beta))\sqrt{\varepsilon}, \tag{3.22}$$

where the constant C_0 is extracted from the solution of the integral equation (3.13) and is given by

$$C_0(\alpha) = \tfrac{1}{2}\int_{\alpha Y}^{Y} d(X)\,dX = \tfrac{1}{2}\int_{\alpha Y}^{Y} X^{-1} f(\log X)\,dX. \tag{3.23}$$

This is independent of the choice of $Y \gg 1$ from (3.16). The interpretation here is that the integral from αY to Y is a measure of how much scalar is being pumped from the mainstream into the boundary layer and lost to the system.

This appears to be as far as one can go analytically. A code was therefore written to solve the boundary layer integral equation (3.13) and obtain the function $d(X)$. The code followed $d(X)$ on a grid, and simply iterated the left-hand side of the integral equation, leading to speedy convergence of $d(X)$. For $\alpha = 0.3$, the solution $d(X)$ obtained is shown in figure 10(a), plotted against X. To confirm that it has the correct large-X behaviour (3.16), in (b) $Xd(X) = f(\log X)$ is plotted against $\log X$. Clearly visible are oscillations of period $\log\alpha \simeq -1.2$.

From the boundary layer solution for a given α, the constant $C_0(\alpha)$ may be extracted by the numerical integration (3.23) of the far field. Adding $C_0(\alpha)$ and $C_0(\beta)$ gives the contribution from the two boundary layers to the scaling law (2.20). Figure 11(a) shows $C_0(\alpha) + C_0(\beta)$ obtained from the boundary layer calculation, plotted against α. For comparison, the quantity $\varepsilon^{-1/2}(\lambda - 1)$ is computed for the upper branches in figure 2(a,b,c), and this is plotted for $\varepsilon = 10^{-3}$ (dot), $\varepsilon = 10^{-4}$ (dash) and $\varepsilon = 10^{-5}$ (dot–dash). These curves converge nicely on the correct theoretical curve as ε is reduced, confirming the theory.

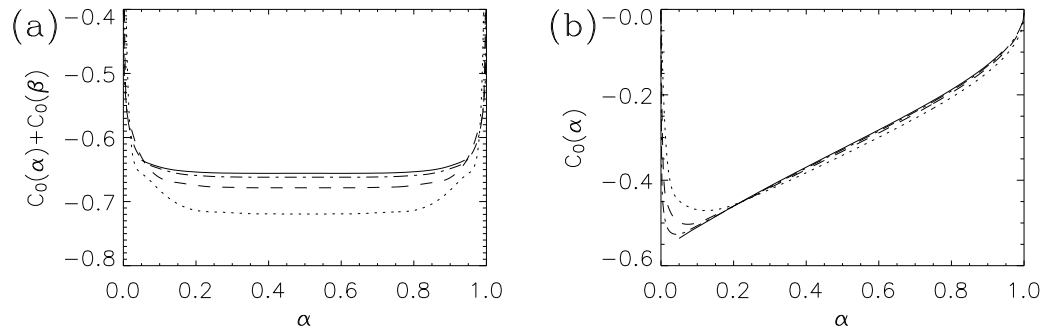

Fig. 11. Comparison of boundary layer calculation. (a) $C_0(\alpha) + C_0(\beta)$ is plotted against α for $0.06 \leq \alpha \leq 0.94$ (solid). Also $\varepsilon^{-1/2}(\lambda - 1)$ is plotted for $\varepsilon = 10^{-3}$ (dot), 10^{-4} (dash) and 10^{-5} (dot–dash) with the (Z) boundary condition. (b) $C_0(\alpha)$ against α for $0.06 \leq \alpha \leq 0.94$ (solid); other curves are as in (a) but for the (ZF) boundary condition.

The quantity $C_0(\alpha) + C_0(\beta)$ is quite flat as a function of α, and so for a further test of the theory, we consider the (ZF) boundary condition, for which the eigenvalue is given by (2.22); the right-hand, no-flux boundary gives a subdominant effect. Figure 11(b) shows $C_0(\alpha)$ plotted against α, and the curves $\varepsilon^{-1/2}(\lambda - 1)$ with data taken from the upper branches of figure 6(a,b,c). Again the collapse onto the theoretical curve is very clear.

4 Eigenvalues and eigenfunctions without diffusion

The analysis of the scalar decay in the last section was based on the constant scalar mode (2.7). As this is the only obvious eigenmode pair we have of T and T^*, we need to develop further machinery to study decay of fluctuations under the no-flux boundary condition and to develop a family of 'strange eigenfunctions'. This involves us with the spectral theory of linear operators [9,10,18,21]; we relegate some technicalities to appendix B, and give an overview in this section.

First suppose that diffusion is non-zero, $\varepsilon > 0$; then T_ε is a compact operator in L^2 and so T_ε and T_ε^* have only point spectrum $\sigma_{\rm p}$, accumulating nowhere except perhaps at zero. For each eigenvalue λ in the point spectrum there is an eigenfunction of T_ε and one of T_ε^*. The eigenvalues are shown schematically in figure 12(a,b) as points marked by $+$ or $*$ in the complex plane. In fact the spectrum depicted schematically is similar to that in figure 4 for the (F) boundary condition, with two leading real eigenvalues ($*$) and some complex conjugate pairs ($+$).

Now suppose we turn off diffusion and consider the operators T and T^* in L^2. These operators lose the key property of compactness (which arises be-

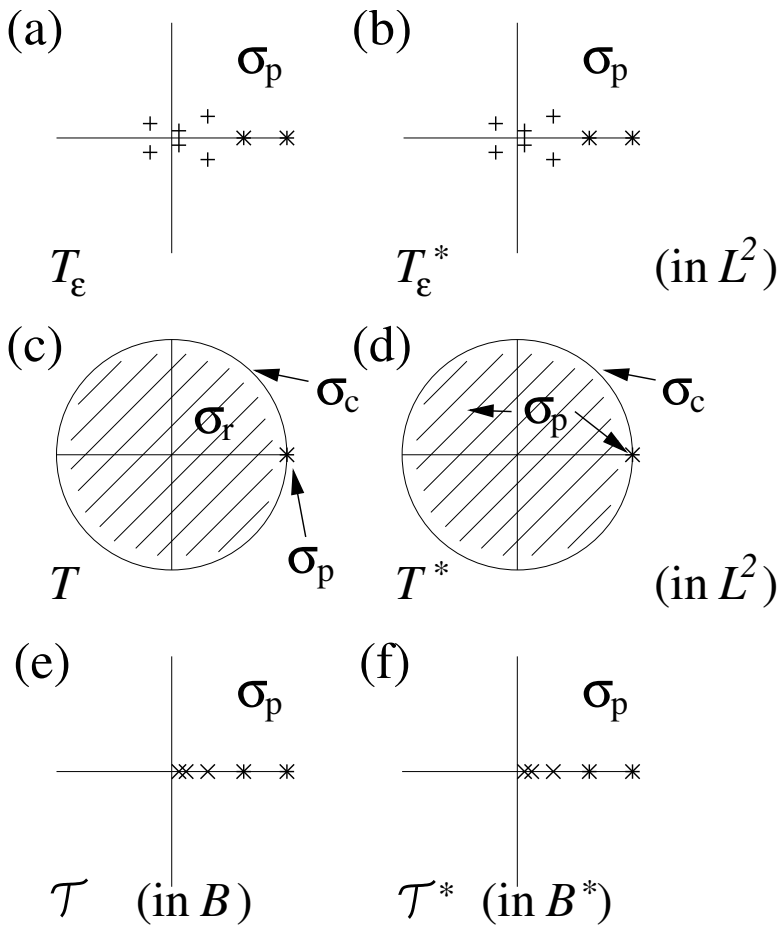

Fig. 12. Schematic picture showing the spectra of various operators in the complex plane for a given value of α: (a) T_ε and (b) T_ε^* in L^2 for a small value of ε, (c) T and (d) T^* in L^2, and (e) $\mathcal{T}$ in $\mathcal{B}$ and (f) $\mathcal{T}^*$ in $\mathcal{B}^*$. σ_p denotes point spectrum, σ_r residual spectrum, and σ_c continuous spectrum.

cause of the effect of diffusion in suppressing small scales for $\varepsilon > 0$), and the corresponding spectra change discontinuously. Appendix B gives the details, which are also summarised in figure 12(c,d). Here we focus only on the point spectrum of T and T^*, that is eigenvalues with corresponding eigenfunctions in L^2.

We have the constant scalar mode (2.7) with $\lambda = 1$ as an eigenvalue of T and T^*; otherwise T has no eigenvalues at all. Perhaps more surprisingly, for T^* *every* λ with $|\lambda| < 1$ is also an eigenvalue. Corresponding eigenfunctions are written down more-or-less explicitly in appendix B; while they lie in L^2, they have structure on every scale and are generally not infinitely differentiable. Our aim is to understand the diffusionless limit of T_ε and T_ε^* and so this large family of eigenfunctions of T^* is not particularly helpful, as members will not generally be robust to diffusion.

However, amongst this large collection of eigenfunctions of T^* are some which

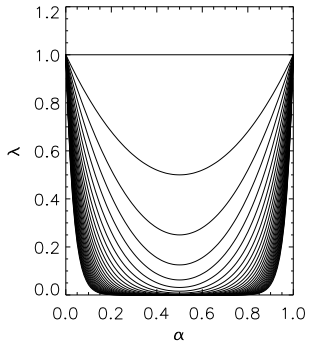

Fig. 13. Eigenvalues $\lambda_{(n)}$ of $\mathcal{T}$ or $\mathcal{T}^*$ as a function of α.

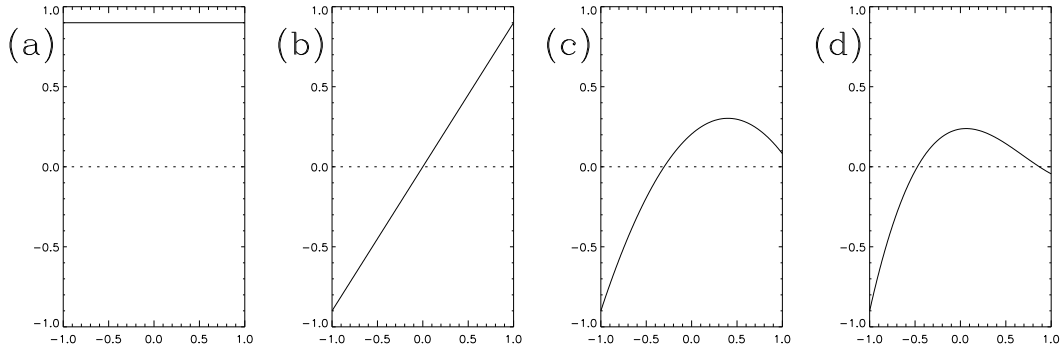

Fig. 14. Leading four eigenfunctions $b_{(n)}$ of $\mathcal{T}^*$ for $\alpha = 0.3$ and zero diffusion; in (a,b,c,d) $n = 0, 1, 2, 3$.

are perfectly well-behaved. Plainly there is a collection of eigenvalues of T^*

$$\lambda_{(n)} = \alpha^{n+1} + \beta^{n+1} \qquad (n \geq 0), \tag{4.1}$$

for which the eigenfunction is simply an nth order polynomial $b_{(n)}$, with

$$b_{(0)} = 1, \quad b_{(1)} = x, \quad b_{(2)} = x^2 + 2\Upsilon x - \tfrac{1}{3}; \tag{4.2}$$

see [10]. Figure 13 shows the eigenvalues $\lambda_{(n)}$ as a function of α, and figure 14 shows the leading four eigenfunctions for $\alpha = 0.3$. These eigenvalues and eigenfunctions of T^* will be used to understand the diffusionless limit of T_ε. Indeed the first non-trivial branch, $\lambda_{(1)}$ in (4.1) is responsible for the decay of fluctuations in the case of the no-flux boundary condition; see (2.21). These eigenvalues (4.1) are also known as Ruelle–Pollicott resonances [20,29,32] and may be obtained using methods based on periodic orbit sums [4,5,33].

While we have these eigenfunctions (4.2) of T^*, to apply perturbation theory we will need to impose solvability conditions, which will mean that we need to have corresponding 'eigenfunctions' of T. This raises issues as these take the form of distributions or 'strange eigenfunctions', lying outside L^2, and to handle this we need a change of viewpoint. We follow [18,33] closely, and these papers should be consulted for further information. The study [20] has a similar

approach and gives the example of a baker's map with even stretching, $\alpha = \beta = 1/2$. We fix any real constant $r > 1$ and consider the space $\mathcal{B}^*$ of complex functions $b(z)$ analytic in the open disc $\mathcal{D} = \{z : |z| < r\}$ and continuous in the closed disc $\overline{\mathcal{D}}$, under the supremum norm, $\|c\| = \sup_{z\in\mathcal{D}} |c(z)|$. This space is a subspace of L^2 and we may restrict [1] the adjoint operator T^* to $\mathcal{B}^*$, calling this restriction $\mathcal{T}^*$. This operator is given by the original formula (2.6), that is,

$$\mathcal{T}^* b(z) = \alpha b(\alpha z - \beta) + \beta b(\beta z + \alpha), \tag{4.3}$$

but has different properties from T^* as it acts in a different space. In particular $\mathcal{T}^*$ is 'analyticity improving': given $b \in \mathcal{B}^*$, the left-hand term of $\mathcal{T}^* b$ is analytic in the disc $|z - \beta/\alpha| < r/\alpha$ and right-hand term in $|z + \alpha/\beta| < r/\beta$. This implies that $\mathcal{T}^* b$ is analytic in the disc

$$|z| < \min((\alpha^{-1}(r - \beta), \beta^{-1}(r - \alpha)) \supset \overline{\mathcal{D}}. \tag{4.4}$$

Because of the analyticity improving property of $\mathcal{T}^*$, any eigenfunction b with non-zero eigenvalue λ is an entire function, as is easily deduced by writing $b = \lambda^{-1}\mathcal{T}^* b$ and applying (4.4) repeatedly.

This analyticity improving property also implies that $\mathcal{T}^*$ is a compact operator from $\mathcal{B}^*$ to itself, and so has point spectrum only, as depicted in figure 12(f). A function $b \in \mathcal{B}^*$ may be expanded as a power series

$$b(z) = \sum_{n=0}^{\infty} b_n z^n. \tag{4.5}$$

The operator $\mathcal{T}^*$ can be considered as a map of coefficients b_n in the above power series, and truncating the power series gives a finite matrix with elements (4.9) below, whose eigenvalues may be found numerically. This was done numerically yielding figure 13, which consists of precisely the branches $\lambda_{(n)}$ in (4.1).

In this way, restricting from L^2 to $\mathcal{B}^*$ and considering $\mathcal{T}^*$ rather than T^*, we obtain a sensible family of eigenfunctions with smoothness properties likely to be useful in considering the limit of weak diffusion. We now consider the adjoint space $\mathcal{B}$ of bounded linear functionals [2] acting on $\mathcal{B}^*$. One convenient way to define $\mathcal{B}$ is to consider a function taking the form

$$a(z) = \sum_{n=0}^{\infty} a_n z^{-n-1} \tag{4.6}$$

[1] In [18] this restriction was called S and the space $\mathcal{B}^*$ was called $\mathcal{B}$.

[2] Strictly this space should be denoted $\mathcal{B}^{**}$ as the adjoint to $\mathcal{B}^*$. Our notation is a little informal so as to be intuitive for the reader.

whose action on a function $b \in \mathcal{B}^*$ is given by

$$\langle a, b\rangle = \frac{1}{2\pi i}\oint_{\partial\mathcal{D}} a(z)b(z)\,dz = \sum_{n=0}^{\infty} a_n b_n. \tag{4.7}$$

So bases of $\mathcal{B}$ and $\mathcal{B}^*$ are given, respectively, by

$$e_n = r^n z^{-n-1}, \quad e_n^* = z^n r^{-n}, \quad \langle e_m, e_n^*\rangle = \delta_{mn}, \tag{4.8}$$

and the matrix elements of $\mathcal{T}^*$ using these bases are

$$\mathcal{T}^*_{mn} \equiv \langle e_m, \mathcal{T}^* e_n^*\rangle = \frac{n!}{m!(n-m)!}\, r^{m-n}\left(\alpha^{m+1}(-\beta)^{n-m} + \beta^{m+1}\alpha^{n-m}\right) \tag{4.9}$$

for $m \le n$, or zero otherwise.

For $a \in \mathcal{B}$ to be a bounded linear functional it must have bounded values when it acts on the basis $\{e_n^*\}$, and from this the coefficients a_n in (4.6) must satisfy that a_n/r^n is bounded. We conclude that $a_n = O(r^n)$ and so in (4.6) $a(z)$ must be analytic in the open complement $\mathbb{C}\setminus\overline{\mathcal{D}}$ of the disc $\mathcal{D}$.

Given this framework we can compute the adjoint operator $\mathcal{T}$ of $\mathcal{T}^*$ via considering

$$\langle a, \mathcal{T}^* b\rangle = \frac{1}{2\pi i}\oint_{\partial\mathcal{D}} a(z)[\alpha b(\alpha z - \beta) + \beta b(\beta z + \alpha)]\,dz. \tag{4.10}$$

A change of variable in each term gives

$$\langle a, \mathcal{T}^* b\rangle = \frac{1}{2\pi i}\oint_{\partial\mathcal{D}} a(\alpha^{-1}(z+\beta))b(z)\,dz + \frac{1}{2\pi i}\oint_{\partial\mathcal{D}} a(\beta^{-1}(z-\alpha))b(z)\,dz, \tag{4.11}$$

where we have used the analyticity of b in $\mathcal{D}$ and of a in $\mathbb{C}\setminus\overline{\mathcal{D}}$ to distort the contours resulting from the change of variables back to $\partial\mathcal{D}$ in each case. From this form we extract the adjoint operator to $\mathcal{T}^*$:

$$\mathcal{T}a(z) = a(\alpha^{-1}(z+\beta)) + a(\beta^{-1}(z-\alpha)). \tag{4.12}$$

Since $\mathcal{T}^*$ is a compact operator, so is $\mathcal{T}$, and they share the same eigenvalue spectrum, as depicted schematically in figure 12(e,f). We need to know about the corresponding eigenfunctions in order to employ solvability conditions, as we did in section 3. Now just as $\mathcal{T}^*$ is analyticity improving, so is $\mathcal{T}$: given a function a in $\mathcal{B}$ and so analytic in $|z| > r$, we have that $\mathcal{T}a$ is analytic in the larger region defined by $|z+\beta| > \alpha r$ and $|z-\alpha| > \beta r$. As $\mathcal{T}$ is iterated the region of analyticity grows, and tends to $\mathbb{C}\setminus[-1,1]$, that is all the complex plane except the real line-segment $[-1,1]$. If a is an eigenfunction of $\mathcal{T}$ with non-zero eigenvalue λ, it then follows that a is analytic in $\mathbb{C}\setminus[-1,1]$, which makes a a *hyperfunction* supported on $[-1,1]$; see the book [35] for

formal definitions and further information. Thus we have identified our strange eigenfunctions as lying in this space of hyperfunctions, which is 'larger' than L^2 and includes distributions, as we will explain below.

By substituting the power series (4.6) into (4.12) we can compute the first few terms of the eigenfunctions of $\mathcal{T}$ corresponding to the eigenvalues $\lambda_{(n)}$ in (4.1),

$$a_{(0)} = z^{-1} + \tfrac{1}{3}z^{-3} + \cdots, \tag{4.13}$$
$$a_{(1)} = z^{-2} - 2\Upsilon z^{-3} + \cdots. \tag{4.14}$$

There is no obstacle to computing these eigenfunctions numerically as left eigenvectors of the matrix for $\mathcal{T}^*$ in (4.9). Generally the nth eigenfunction is a power series in z^{-1} starting with the term z^{-n-1},

$$a_{(n)} = z^{-n-1} - (n+1)\,\frac{\alpha^n - \beta^n}{\alpha^n + \beta^n}\, z^{-n-2} + \cdots. \tag{4.15}$$

Given any power series $a(z)$ in (4.6) with this property that $a_0 = a_1 = \cdots = a_{n-1} = 0$, $\mathcal{T}a$ has the same property and this gives a convenient means of specifying the above eigenfunctions as a limit

$$a_{(n)} = \lim_{m\to\infty} \lambda_{(n)}^{-m} \mathcal{T}^m z^{-n-1}. \tag{4.16}$$

It may be checked that, with this definition

$$\langle a_{(m)}, b_{(n)} \rangle = \delta_{mn}. \tag{4.17}$$

Explicitly we have a formula

$$a_{(0)} = \tfrac{1}{2}\log[(z+1)/(z-1)], \tag{4.18}$$

as is easily confirmed. For $\alpha = \beta = \frac{1}{2}$ only the remaining eigenfunctions are simply derivatives of this, up to normalisation,

$$2n a_{(n)} = (z-1)^{-n} - (z+1)^{-n} \quad (n \geq 1). \tag{4.19}$$

Finally, just as we restricted T^* to $\mathcal{B}^* \subset L^2$ to obtain $\mathcal{T}^*$, with pleasanter properties, it is worth relating $\mathcal{B}$ to L^2 and $\mathcal{T}$ to T. To do this we first note that given any function a in L^2 we can define a hyperfunction $\mathcal{F}a$ by

$$\mathcal{F}a(z) = \int_{-1}^{1} \frac{a(x)}{z-x}\, dx; \tag{4.20}$$

here the information in $a(x)$ is coded into the lack of analyticity of $\mathcal{F}a$ along the line segment $[-1, 1]$. With this definition it is clear that for $a \in L^2$, and $b \in \mathcal{B}^* \subset L^2$

$$\mathcal{T}\mathcal{F}a = \mathcal{F}Ta, \quad \langle \mathcal{F}a, b \rangle = (a, b), \tag{4.21}$$

the latter being just the L^2 inner product (2.4). As an example of this, we can see that the leading eigenfunction (4.18) of $\mathcal{T}$ is just the constant scalar mode (2.7) mapped into $\mathcal{B}$ by means of (4.20).

In this way we can consider members of L^2 as being naturally embedded as hyperfunctions, lying in $\mathcal{B}$, and then the actions of $\mathcal{T}$ in $\mathcal{B}$ and T in L^2 correspond; indeed this is suggested by the close similarity of (2.3) and (4.12). However the space $\mathcal{B}$ is rather larger than L^2, and includes distributions on $[-1,1]$ [35]. So, for example, a delta function distribution at $y \in [-1,1]$ is given by

$$a(x) = \delta(x-y), \quad \mathcal{F}a(z) = (z-y)^{-1}, \tag{4.22}$$

and for the nth derivative of a delta function,

$$a(x) = (-1)^n \frac{d^n\delta}{dx^n}(x-y), \quad \mathcal{F}a(z) = n!\,(z-y)^{-n-1}. \tag{4.23}$$

Thus in the special case $\alpha = \beta = \frac{1}{2}$ the eigenfunctions (4.19) correspond to distributions,

$$a_{(n)} = \frac{(-1)^{n-1}}{2n!}\left(\frac{d^{n-1}\delta}{dx^{n-1}}(x-1) - \frac{d^{n-1}\delta}{dx^{n-1}}(x+1)\right) \qquad (n \geq 1), \tag{4.24}$$

localised at each endpoint. Similar results apply in the dynamo problem; see §9.5.2 of [10], [30,18].

This also means we can understand an eigenfunction $a_{(n)}$ (4.16) in the sense of a distribution. For a given m the quantity $\lambda_{(n)}^{-m}\mathcal{T}^m z^{-n-1}$ is a complex function with 2^m poles of order $n+1$, with certain weights attached. Each pole lies on $[-1,1]$ and corresponds to the nth derivative of a delta function. To formalise this, define sets W_m for $m \geq 0$ of pairs (y,w) of points y and weights w recursively, by $W_0 = \{(0,1)\}$ and

$$W_m = \{(\alpha y - \beta, \alpha^{n+1}\lambda_{(n)}^{-1}w), (\beta y + \alpha, \beta^{n+1}\lambda_{(n)}^{-1}w) : (y,w) \in W_{m-1}\}. \tag{4.25}$$

With this we can rewrite the eigenfunction $a_{(n)}$ using the form (4.16) as a limiting sum of nth derivative delta functions

$$a_{(n)}(x) = \lim_{m\to\infty} \sum_{(y,w)\in W_m} (-1)^n \frac{w}{n!}\frac{d^n\delta}{dx^n}(x-y). \tag{4.26}$$

Its action on a function $b \in \mathcal{B}^*$ is given by

$$(a_{(n)}, b) = \langle \mathcal{F}a_{(n)}, b\rangle = \lim_{m\to\infty} \sum_{(y,w)\in W_m} \frac{w}{n!}\frac{d^n b}{dx^n}(y). \tag{4.27}$$

In the case when $n = 0$, this in fact corresponds to integrating $b(x)$ multiplied by $\frac{1}{2}$ over the line segment $[-1,1]$, in keeping with (2.7) or (4.18). For $n \geq 1$

there is no obvious interpretation, except in the special case $\alpha = \beta = 1/2$, when all the weights w are equal and points y equally spaced, giving

$$(a_{(n)}, b) = \frac{1}{2n!} \int_{-1}^{1} \frac{d^n b}{dx^n}\, dx, \tag{4.28}$$

in agreement with (4.24); see §9.5.2 of [10].

In conclusion, we find that the theory developed in this section has led us to a nicely symmetrical situation. Referring to figure 12, on the right-hand side restricting our space from (d) L^2 to (f) $\mathcal{B}^*$ allows us to select key well-behaved eigenfunctions of $\mathcal{T}^*$ that may be relevant when we introduce diffusion. On the left-hand side, expanding our space from (c) L^2 to (e) $\mathcal{B}$, means that instead of having no eigenfunctions bar (2.7) in L^2, we have a set of well-defined (strange) eigenfunctions, now taking the form of distributions, lying in $\mathcal{B}$ but not corresponding to functions in L^2.

5 Scalar decay with the no-flux boundary condition

We now return to the problem of scalar decay with weak diffusion, focussing particularly on the no-flux boundary condition. The key result we need from the last section is the identification of the set of eigenvalues (4.1) with well-behaved eigenfunctions (4.2) of $\mathcal{T}^*$ and the set of distributional eigenfunctions (4.26) of $\mathcal{T}$, all for zero diffusion.

These eigenvalues of $\mathcal{T}$ and $\mathcal{T}^*$ are depicted schematically in figure 12(e,f); in some cases these diffusionless eigenvalues may be close to eigenvalues in the spectrum of T_ε and T_ε^* for small diffusion ε, shown in 12(a,b). In other cases there may be no link. Some terminology (broadly in line with [10]) may be helpful:

(i) A *perfect mode* is an eigenfunction pair of $\mathcal{T}$ and $\mathcal{T}^*$ with eigenvalue $\lambda \neq 0$ (shown as $\times$ or $\ast$ in figure 12(e,f)).
(ii) We call such a perfect mode *robust* to diffusion ($\ast$ in 12(e,f)) if there is an eigenvalue λ_ε of T_ε and T_ε^* with $\lambda_\varepsilon \to \lambda$ as $\varepsilon \to 0$. The corresponding limiting eigenfunction pair of T_ε and T_ε^* is called *non-diffusive* ($\ast$ in 12(a,b)).
(iii) A perfect mode which is not robust is called *delicate*, being entirely destroyed by diffusion, no matter how weak ($\times$ in 12(e,f)).
(iv) A mode of T_ε that fails to be non-diffusive is called *diffusive*; it owes its existence entirely to diffusion and does not have a perfect mode counterpart ($+$ in 12(a,b))

The idea is that for a robust perfect mode, weak diffusion gives only a small

perturbation, and links the perfect mode to a non-diffusive mode of T_ε and T_ε^* for small ε. This terminology is plainly somewhat informal, as it does not consider ways in which eigenvalues might accumulate in the limit $\varepsilon \to 0$ (and such accumulation is visible in the lower branches of figures 2, 4, 6 and 8). Also we should note that the above properties depend on the boundary condition employed, and the value of α. For example, in figure 13 the leading perfect branch $\lambda_{(0)} = 1$ is robust for all boundary conditions, whereas the next perfect branch $\lambda_{(1)} = \alpha^2 + \beta^2$ is robust for the (F) boundary condition, and for the (ZF) boundary condition for $\alpha < 1/2$ but delicate otherwise (see figures 2, 4, 6 and 8).

In this section we have two aims: the first is to obtain criteria for when a perfect mode will be robust or be delicate. If such a mode has eigenvalue λ for a given value of α and $\beta = 1 - \alpha$, we will establish that the mode is robust provided

$$\lambda_0 > \max(\alpha, \beta) \qquad \text{(Z) or (P)}, \tag{5.1}$$
$$\lambda_0 > \max(\alpha^2, \beta^2) \qquad \text{(F)}, \tag{5.2}$$
$$\lambda_0 > \max(\alpha, \beta^2) \qquad \text{(ZF)}. \tag{5.3}$$

These criteria are in good accord with the numerical results of section 2, comparing with the perfect modes of figure 13.

Our second aim is to establish the decay rate formula (2.21) for the no-flux boundary condition in the limit of weak diffusion. We will take a pragmatic approach, dropping the distinction between $\mathcal{T}$ and T, $\mathcal{T}^*$ and T^*, and not be too concerned about the space in which we are working. In particular whereas the distributional eigenfunctions (4.26) were defined with reference to their action on analytic functions (in $\mathcal{B}^*$), we will apply these distributions to functions whose analyticity properties are unknown. This is justified on the basis that we will obtain formulae that we can confirm numerically.

Our general approach is to follow through the approximations in section 3, equations (3.1)–(3.3), but instead of using the constant scalar mode (2.7), we set $\lambda_0 = \lambda_{(1)}$, $b_0 = b_{(1)}$ and $a_0 = a_{(1)}$, given in (4.1), (4.2) and (4.26), with (4.17) holding. This starting point is motivated by the similarity of figures 5(c) and 14(b). The approximate eigenvalue equation remains (3.4). In the left-hand boundary layer the source term becomes

$$T_1^* b_0(-1 + \sqrt{\varepsilon} X) = 2\sqrt{\varepsilon}\alpha g_1(\alpha X), \tag{5.4}$$

in place of (3.11), with

$$g_1(s) = -s g_0(s) + 2g(s), \qquad g_1'(s) = -g_0(s) \tag{5.5}$$

(see (3.9)). The boundary layer is now weaker, of magnitude $\varepsilon^{1/2}$ and instead

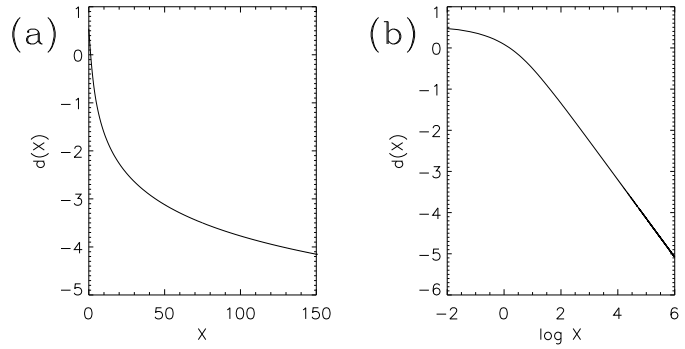

Fig. 15. Solution to boundary layer integral equation (5.7), showing (a) $d(X)$ against X, and (b) $d(X)$ against $\log X$.

of (3.14) we set

$$b_1(-1+\sqrt{\varepsilon}X) = \sqrt{\varepsilon}d(X) \tag{5.6}$$

in the boundary layer, giving an integral equation

$$2\alpha g_1(\alpha X) + \alpha\int_0^\infty [g(\alpha X - Y) + g(\alpha X + Y)]d(Y)\,dY + 2C_1 = \lambda_0 d(X), \tag{5.7}$$

in place of (3.13), with

$$2\sqrt{\varepsilon}C_1 = \beta b_1(\Upsilon) - \lambda_1 b_0(-1). \tag{5.8}$$

Here we have made no assumptions about the size of b_1 or λ_1 and so have retained terms $\beta b_1(\Upsilon)$ (see (3.12)) and $\lambda_1 b_0$ (see (3.4)).

5.1 Even stretching

We begin with the case $\alpha = \beta = 1/2$, of even stretching. By symmetry the solution for b_1 must be an odd function of x and so $b_1(\Upsilon) = b_1(0) = 0$ drops out of (5.8). However it turns out that we cannot drop the term in (5.8) involving λ_1. Instead we need to retain C_1 in (5.7) since this integral equation is degenerate for $\alpha = \lambda_0 = \frac{1}{2}$: given a solution for d, adding a constant to d gives another solution. Together with this goes a solvability condition: numerically it is found that a solution only exists when C_1 takes a certain value and this fixes the correction λ_1, with

$$\lambda_1 = 2C_1(\alpha)\varepsilon^{q(\alpha)}, \quad C_1(\alpha) \simeq -0.16287, \quad q(\alpha) = 1/2 \quad (\alpha = 1/2), \tag{5.9}$$

which is of the form (2.21), mentioned at the outset. The resulting boundary layer has a logarithmic tail

$$d(X) = -4C_1 \log X/\log\alpha + f(\log X), \quad (f \text{ periodic, period } \log\alpha), \tag{5.10}$$

as is seen in figure 15. Confirmation of the results in (5.9) is given below in figure 17(a).

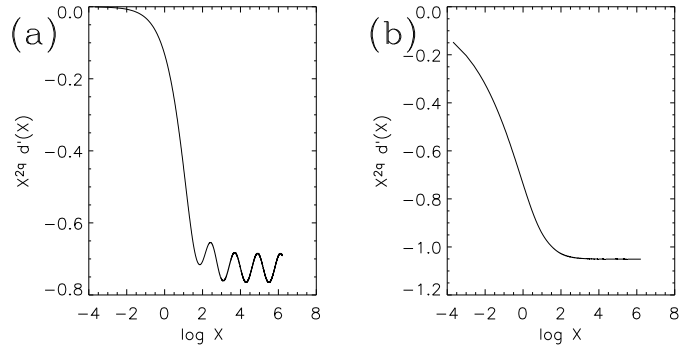

Fig. 16. Solution to boundary layer integral equation (5.12), showing $X^{2q}d'(X)$ against $\log X$ for (a) $\alpha = 0.3$ and (b) $\alpha = 0.7$.

5.2 Uneven stretching

For the case $\alpha \neq \beta$ a change of tack is worthwhile. The calculations will use a solvability condition as we did in section 3 for the (Z) boundary condition. This will involve integrating b_1 against the distribution $a_0 = a_{(1)}$ defined in (4.26). To do this integration, however, we do not need to know b_1 itself, but only its derivative b_1'. For this reason (and others) it is best to work with b_1' directly.

Therefore, suppose we have an eigenvalue and eigenfunction, $T_\varepsilon^* b \equiv T^* H_\varepsilon b = \lambda b$ with the no-flux boundary condition incorporated in H_ε (lower sign in (2.14)). Then b' satisfies $T_\varepsilon'^* b' \equiv T'^* H_\varepsilon b' = \lambda b'$, where

$$T'^* b'(x) = \alpha^2 b'(\alpha x - \beta) + \beta^2 b'(\beta x + \alpha), \tag{5.11}$$

and where now the zero boundary condition (upper sign in (2.14)) is employed in the definition of H_ε. This reformulation is exact, and has the advantage that we eliminate the constant scalar mode (2.7) from consideration. [3]

We can now go through the calculations analogous to (3.4)–(3.13), with dashes everywhere, to obtain the integral equation,

$$-2\alpha^2 g_0(\alpha X) + \alpha^2 \int_0^\infty [g(\alpha X - Y) - g(\alpha X + Y)] d'(Y)\, dY = \lambda_0 d'(X), \tag{5.12}$$

where

$$b_1'(-1 + \sqrt{\varepsilon} X) = d'(X). \tag{5.13}$$

Of course this integral equation is simply the derivative of (5.7). It is based on the assumptions that b_1' decays from the boundary layer into the mainstream,

[3] Note that in L^2 in this case, $\|T'^*\| = \alpha^2 + \beta^2$ and $\|H_\varepsilon\| = e^{-\varepsilon\pi^2/4}$, and so this also gives a rigorous upper bound on the decay of fluctuations, $|\lambda| \leq e^{-\varepsilon\pi^2/4}(\alpha^2 + \beta^2)$.

and that $\lambda_1 \to 0$ as $\varepsilon \to 0$, which we will verify below. In the far field

$$d'(X) = X^{-2q} f(\log X), \quad 2q(\alpha) \equiv 2 - \frac{\log \lambda_0}{\log \alpha}, \quad (f \text{ periodic, period } \log \alpha). \tag{5.14}$$

Note that q is real (contrast the case in section 7 below) and that it is positive, under the conditions for robustness we stated above in (5.2). The boundary layer equation (5.12) was solved numerically on a grid by simply iterating the left-hand side, and the results are shown in figure 16, which confirms this large-X behaviour.

Now we need to link the boundary layer to the mainstream in the overlap region $1 \ll X \ll \varepsilon^{-1/2}$. If we follow the argument in section 3 from (3.17) to (3.20) using undashed variables we obtain as the analogue of (3.21),

$$\lambda_{1\mathrm{L}} = \lambda_0 \int_{-1+\alpha\mu}^{-1+\mu} a_0 b_1 \, dx \tag{5.15}$$

for the contribution from the left-hand boundary layer. The problem is that a_0 is the distribution (4.26) with $n = 1$. To manipulate this into a useful form we first set, without loss of generality, $\mu = 2\alpha^p$, so that the interval is over the range $[-1 + 2\alpha^{p+1}, -1 + 2\alpha^p]$, in the overlap region.

Next we use the property that a_0 is an eigenfunction of T, in the sense of a distribution satisfying $Ta_0 = \lambda_0 a_0$. For x in the range $-1 \le x \le \Upsilon$ this gives that

$$a_0(x) = \lambda_0^{-1} a_0(\alpha^{-1}(x + \beta)). \tag{5.16}$$

If we substitute this into (5.15) and change variable from x to $\alpha^{-1}(x+\beta)$ this gives

$$\lambda_{1\mathrm{L}} = \lambda_0 \frac{\alpha}{\lambda_0} \int_{-1+2\alpha^p}^{-1+2\alpha^{p-1}} a_0(x) b_1(\alpha(x+1) - 1) \, dx. \tag{5.17}$$

If this process is repeated a total of p times we end up with

$$\lambda_{1\mathrm{L}} = \lambda_0 \frac{\alpha^p}{\lambda_0^p} \int_{\Upsilon}^{1} a_0(x) b_1(\alpha^p(x+1) - 1) \, dx. \tag{5.18}$$

Setting for the moment $\tilde{a}_0$ as the integral of $a_0 = a_{(1)}$ in (4.26), that is

$$\tilde{a}_0(x) = \lim_{m\to\infty} \sum_{(y,w)\in W_m} -w \, \delta(x - y), \tag{5.19}$$

and using (5.13) allows us to rewrite this as

$$\lambda_{1\mathrm{L}} = \lambda_0 \frac{\alpha^{2p}}{\lambda_0^p} \int_{\Upsilon}^{1} -\tilde{a}_0(x) d'(\alpha^p(x+1)/\sqrt{\varepsilon}) \, dx. \tag{5.20}$$

Finally substituting in for the far field of $d'(X)$ from (5.14) and using the

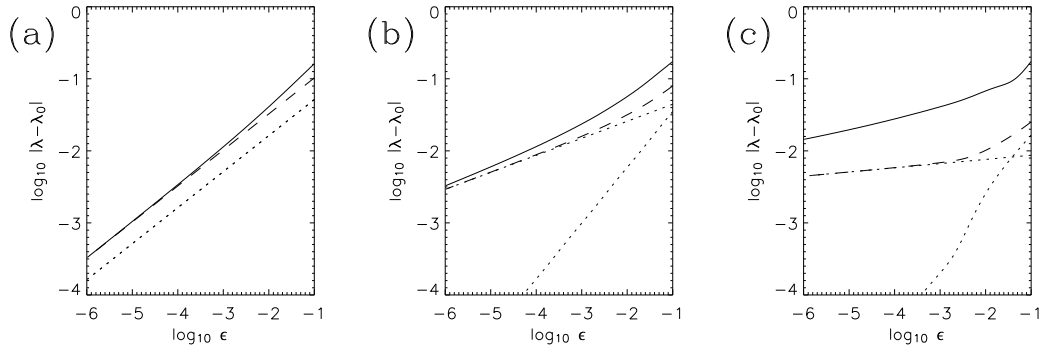

Fig. 17. Comparison of boundary layer theory and numerical simulations for the (F) boundary condition; plotted is $\log_{10}|\lambda-\lambda_0|$ against $\log_{10}\varepsilon$ (solid). Also shown are the asymptotic contributions from left- (see (5.21)) and right-hand boundary layers (dotted) and their sum (dashed). In (a) $\alpha=0.5$, (b) $\alpha=0.3$, and (c) $\alpha=0.1$.

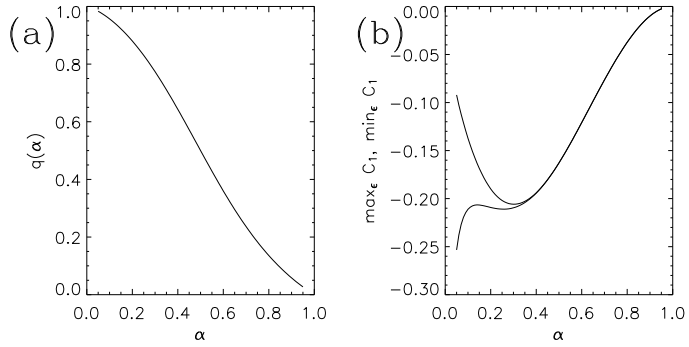

Fig. 18. (a) The exponent $q(\alpha)$ is plotted against α. (b) Plot against α of the maximum and minimum values of $C_1(\alpha,\varepsilon)$ for varying ε.

definition of q yields the left-hand contribution as

$$\lambda_{1\mathrm{L}} = C_1(\alpha,\varepsilon)\varepsilon^{q(\alpha)}, \tag{5.21}$$

with

$$C_1(\alpha,\varepsilon) = \lambda_0 \int_\Upsilon^1 -\tilde{a}_0(x)(x+1)^{-2q} f(\log(x+1) - \tfrac{1}{2}\log\varepsilon)\,dx, \tag{5.22}$$

that is,

$$C_1(\alpha,\varepsilon) \equiv \lambda_0 \lim_{m\to\infty} \sum_{(y,w)\in W_m, y>\Upsilon} w\,(y+1)^{-2q} f(\log(y+1) - \tfrac{1}{2}\log\varepsilon). \tag{5.23}$$

Combining the right-hand boundary layer gives us (2.21) and we have identified the exponents q in (5.14). The 'constant' C_1 has period $\log\alpha$ in the variable $\frac{1}{2}\log\varepsilon$.

To confirm our theory, for a given α we compute the solution to the integral equation (5.12). Using data for large X, we can then compute $C_1(\alpha,\varepsilon)$ for a given value of ε by evaluating the sum (5.23) for a reasonable value of m (say

up to $m = 20$). This gives the contribution from the left-hand boundary layer, and with a similar contribution from the right-hand boundary layer we obtain our asymptotic approximation; this is shown as dashed curves in figure 17, with the full numerical results shown solid. The results for $\alpha = \beta = 0.5$ in (a) correspond to those found earlier in (5.9). For $\alpha = 0.3$, $\beta = 0.7$ in (b), the right-hand boundary layer gives the dominant contribution, and clear convergence of the numerical results is seen as $\varepsilon \to 0$. In (c) for $\alpha = 0.1$ and $\beta = 0.9$ convergence is much slower, but this is unsurprising given the shallowness of the power law dependence generated by the right-hand boundary layer.

Figure 18 shows $q(\alpha)$ and the maximum and minimum values of C_1 (for varying diffusivity ε), plotted against α. Note that $C_1(\alpha, \varepsilon)$ is in fact constant as a function of ε for $\alpha \geq 1/2$, as far as we can tell numerically; we have no particular theoretical reason why this should be the case (except when $\alpha = \beta = 1/2$ in section 5.1 above). Since for $\alpha < \beta$, say, the right-hand boundary layer dominates, and is controlled by $q(\beta)$ and the constant $C_1(\beta, \varepsilon)$, oscillations in C_1 are never really visible in the total correction λ_1. This may be contrasted with the situation for the stretch–fold map in section 7 below.

We also obtain from our analysis straightforward criteria for the robustness of perfect branches (recalling the definitions at the beginning of this section). For the above perturbation theory to make sense we require $q > 0$, otherwise the 'correction' (5.21) diverges as $\varepsilon \to 0$, and we conclude that diffusion is sufficiently strong that the boundary layers overwhelm the perfect branch. This gives the criterion in (5.2). This is for the (F) boundary condition, where boundary layers of magnitude $O(\sqrt{\varepsilon})$ are triggered, from (5.4). For the case of a (Z) or (P) boundary condition the layers are of magnitude $O(1)$ from (3.11), and so the corresponding value of $q(\alpha)$ is given by $2q = 1 - \log \lambda_0 / \log \alpha$. Requiring $q > 0$ for left- and right-hand boundary layers gives the criteria (5.1) and (5.3) for robustness.

6 Scalar decay with the periodic boundary condition

The case of the periodic boundary condition (P) has some distinct features from the (Z) and (F) cases considered above. First of all there is no obvious link between the branches of T_ε depicted in figure 8 and the perfect modes of $\mathcal{T}$ shown in figure 13. Except for the branch with $\lambda = 1$, the branches of T_ε therefore count as diffusive modes, in the terminology of section 5, that decay more slowly than the non-constant perfect modes. The eigenvalues of T_ε also come in complex conjugate pairs, and appear to accumulate on the curve $|\lambda| = \max(\alpha, \beta)$ as $\varepsilon \to 0$. However they converge rather slowly with ε, suggesting that powers of $\log \varepsilon^{-1}$ are involved [14,37].

Our aim is to understand these features and provide analysis for small ε. To begin with note that the adjoint eigenfunctions for $\alpha = 0.3$, with diffusion, in figure 9(c,d), show smooth behaviour in the mainstream, but then some rapid variation in the boundary layers, especially the right-hand one, $x \simeq 1$. This indicates that the mode is likely to be 'driven' by the boundary layers, and we should seek a solution in which these 'control' the mainstream (in contrast to the (Z) and (F) cases, where a perfect mode, if robust, exists in the mainstream and drives the boundary layers).

Suppose we have an eigenfunction, $T_\varepsilon^* b = \lambda b$. Then a key quantity we will need is

$$\Delta = b(1) - b(-1). \tag{6.1}$$

The quantity $-\Delta$ is the jump in b at the ends of the interval if we imagine b to be periodically extended in space. Assuming $\Delta \neq 0$, we are free to normalise an eigenfunction so that $\Delta = 1$. Imagine taking such an eigenfunction and apply H_ε: this will smooth out the jump in a boundary layer of scale $\sqrt{\varepsilon}$ with negative gradients of magnitude $\varepsilon^{-1/2}$. Applying T^* again to give λb will generate a new jump, of size $-\lambda\Delta$. It is this continual creation of fine scales at the boundaries that enables a slowly-decaying eigenfunction to 'live' there, and control the mainstream.

In terms of analysis it is convenient to work with the derivative $b'(x)$ of our eigenfunction (for $-1 < x < 1$). Differentiating $T^* H_\varepsilon b = \lambda b$ and using $\Delta = 1$ gives

$$T'^* H_\varepsilon b'(x) - [\alpha^2 G_\varepsilon(\alpha(x+1)) + \beta^2 G_\varepsilon(\beta(x-1))] = \lambda b'(x). \tag{6.2}$$

Here T'^* is given in (5.11) and there is no approximation beyond taking ε small so that we neglect terms in (2.15) that give only exponentially small effects. The terms involving G_ε arise from diffusion acting on the jump $-\Delta = -1$. This equation is to be solved for $b'(x)$ subject to the integral constraint

$$\Delta \equiv \int_{-1}^{1} b'(x)\, dx = 1. \tag{6.3}$$

Again we consider a boundary layer problem; define $d'(X)$ by

$$b'(-1 + \sqrt{\varepsilon}X) = \varepsilon^{-1/2} d'(X) \qquad (X > 0), \tag{6.4}$$

$$b'(1 + \sqrt{\varepsilon}X) = \varepsilon^{-1/2} d'(X) \qquad (X < 0) \tag{6.5}$$

in the left- (L) and right-hand (R) boundary layers respectively, and then (6.2) becomes

$$\alpha^2 \int_{-\infty}^{\infty} g(\alpha X - Y) d'(Y)\, dY - \alpha^2 g(\alpha X) = \lambda d'(X) \qquad (X > 0),$$

$$\beta^2 \int_{-\infty}^{\infty} g(\beta X - Y) d'(Y)\, dY - \beta^2 g(\beta X) = \lambda d'(X) \qquad (X < 0). \tag{6.6}$$

Here we have neglected a term involving $b'(\Upsilon)$ since b' is weaker in the mainstream than in the boundary layers, as we shall see.

The far field behaviour of the solution to this integral equation is given by

$$d'(X) = X^{-2q_{\mathrm{L}}} f_{\mathrm{L}}, \quad 2q_{\mathrm{L}} \equiv 2 - \frac{\log\lambda}{\log\alpha}, \qquad (X > 0, X \gg 1), \tag{6.7}$$

$$d'(X) = (-X)^{-2q_{\mathrm{R}}} f_{\mathrm{R}}, \quad 2q_{\mathrm{R}} \equiv 2 - \frac{\log\lambda}{\log\beta}, \qquad (X < 0, X \gg 1). \tag{6.8}$$

Here f_{L} and f_{R} are, generally, functions of $\log X$ with periods $\log\alpha$ and $\log\beta$, respectively.

These decaying tails will drive a solution in the mainstream. It is convenient to take $\alpha < \beta$ (without loss of generality, as if $\alpha = \beta = 1/2$ we know that super-exponential decay occurs). In this case the right-hand boundary layer given by $d'(X)$ for $X < 0$, decays most slowly into the mainstream, and so is dominant. Also we find numerically that f_R is actually constant when the integral equation (6.6) is solved, and so will drop any dependence of f_R on $\log X$ (see figure 20 below). In the mainstream we set

$$b'(x) \equiv \varepsilon^{q_{\mathrm{R}}-1/2} f_{\mathrm{R}} b'_{\mathrm{ms}}(x), \tag{6.9}$$

where

$$T'^{*} b'_{\mathrm{ms}} = \lambda b'_{\mathrm{ms}} \tag{6.10}$$

at leading order. This must match onto the far field of the right-hand boundary layer,

$$b'_{\mathrm{ms}} \sim b'_{\mathrm{sing}}(x), \qquad b'_{\mathrm{sing}}(x) \equiv (1-x)^{-2q_{\mathrm{R}}}, \tag{6.11}$$

as $x \to 1$.

Interestingly we can now see why eigenvalues λ will be complex in this periodic case. Suppose λ is real and positive, and imagine solving the integral equation (6.6) by iteration of the left-hand side. Since the source terms involving g are wholly negative, the solution $d'(X)$ that is developed will also be negative everywhere. The far field tails that arise from the stretching action of T'^{*} will also be negative with $f_{\mathrm{L}}, f_{\mathrm{R}} < 0$. These then must drive a mainstream solution which is again everywhere negative, as in the mainstream the action of T'^{*} is of stretching out and averaging. The result will be that $b'(x)$ will be negative across the whole interval, and it is then impossible to satisfy (6.3). The conclusion is that λ real and positive is impossible, and λ must be complex or negative. In either case the decay of the passive scalar with the (P) boundary condition would be oscillatory as seen.

Now let us consider how this problem can be avoided. If λ is, say, negative, then there will be an oscillations, with complex q_{L}, q_{R} in (6.7), (6.8) (cf. section 7.2 below) and this would make it easier to satisfy $\Delta = 1$. However this will

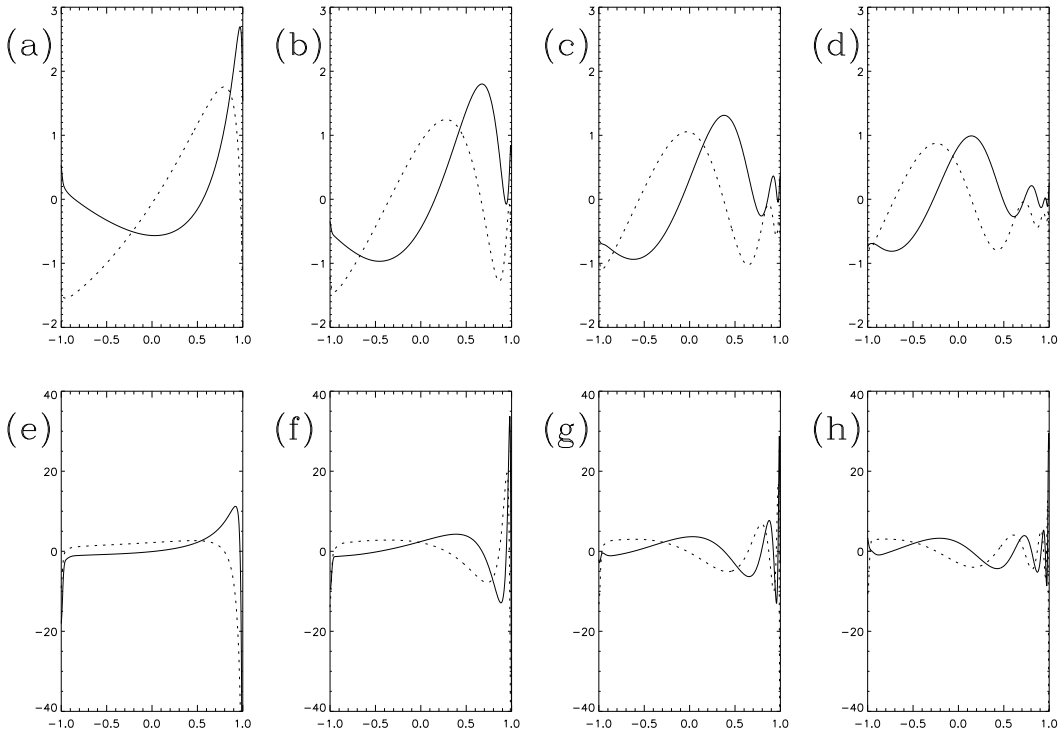

Fig. 19. (a–d) show the leading non-constant eigenmodes b of T_ε^* for the (P) boundary condition with $\varepsilon = 10^{-5}$ and $\alpha = 0.3$, normalised by $\Delta = 1$. (e–h) show the corresponding derivatives b'.

also imply stronger diffusive damping in the boundary layer and reduce λ. The best way in which $\Delta = 1$ can be satisfied for the least diffusive penalty is to put λ close to the real line, but just far enough off it that the oscillation in the exponent $\varepsilon^{q_R - 1/2}$ in the tail (6.8) allows a change of sign of b' in the mainstream. For this effect to give a contribution of order unity to Δ, (and not too large) we require that $\operatorname{Re} q_R \sim 1/2$ as $\varepsilon \to 0$. Also, for $\varepsilon^{q_R - 1/2}$ to change sign, we require the imaginary part of q_R to be of order $n(\log \varepsilon^{-1})^{-1}$, where n counts the number of sign changes. Thus we obtain a very basic estimate

$$\lambda = \beta + o(\varepsilon), \qquad q_R = \tfrac{1}{2} + o(\varepsilon), \tag{6.12}$$

or more precisely we might expect

$$\lambda = \beta + O(in(\log \varepsilon^{-1})^{-1}), \qquad q_R = \tfrac{1}{2} + O(in(\log \varepsilon^{-1})^{-1}). \tag{6.13}$$

This argument, although somewhat informal, gives much of what we see numerically in figure 8, in particular the slow convergence to $\lambda = \beta$, the complex eigenvalues, and the slow accumulation of branches.

We will flesh out this argument in what follows, but to confirm that it is broadly correct, figure 19(a–d) shows eigenmodes $b(x)$ (one per complex pair of eigenvalues), normalised by $\Delta = 1$, and (e–h) shows their derivatives $b'(x)$.

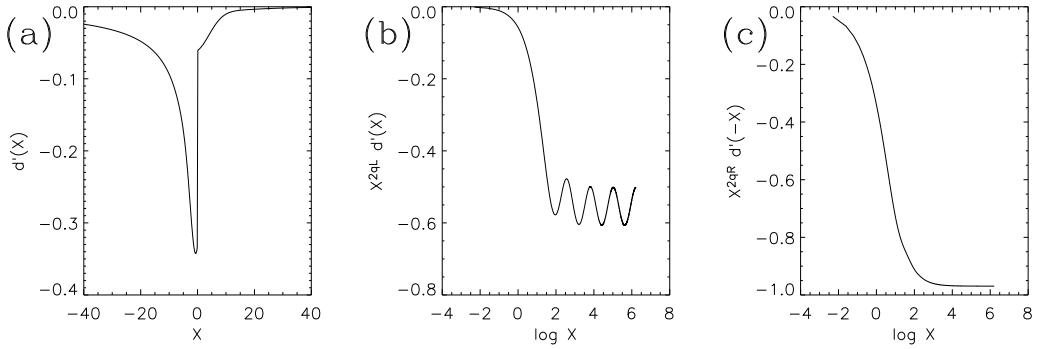

Fig. 20. Solution to boundary layer integral equation (6.6), showing (a) $d'(X)$ against X, (b) $X^{2q_{\rm L}}d'(X)$ against $\log X$, and (b) $X^{2q_{\rm R}}d'(-X)$ against $\log X$.

We see clearly that the nth eigenfunction has n peaks in b' corresponding to increasing numbers of changes of sign, going in to the mainstream from the right-hand boundary layer.

Returning to the mainstream, we require a solution of (6.10) with (6.11) holding. Now if we apply $\lambda^{-1}T'^*$ to $b'_{\rm sing}$ we obtain the same singular solution at $x = 1$, and another term which is regular in $[-1, 1]$,

$$\lambda^{-1}T'^* b'_{\rm sing} = b'_{\rm sing} + \lambda^{-1}\alpha^{2-2q_{\rm R}}(\alpha^{-1}(1+\beta) - x)^{-2q_{\rm R}}. \tag{6.14}$$

The second term is bounded in $[-1, 1]$ only having a singularity further along the real line. If we iterate this process, we can write down the mainstream solution as a limit

$$b'_{\rm ms} = \lim_{n\to\infty} \lambda^{-n}(T'^*)^n b'_{\rm sing} \equiv b'_{\rm sing} + b'_{\rm conv}, \tag{6.15}$$

where $b'_{\rm conv}$ is well-behaved in $[-1, 1]$ and is given by the sum

$$b'_{\rm conv} = \sum_{(y,w)\in V_\infty, y\neq 1} w(y-x)^{-2q_{\rm R}}, \tag{6.16}$$

which is geometrically convergent for small ε given (6.12) and $\alpha < \beta$. Here we have defined points and weights (y, w) recursively, by $V_0 = \{(1, 1)\}$,

$$V_m = \{(\alpha^{-1}(y+\beta), \alpha^{2-2q_{\rm R}}\lambda^{-1}w), (\beta^{-1}(y-\alpha), \beta^{2-2q_{\rm R}}\lambda^{-1}w) : (y, w) \in V_{m-1}\}, \tag{6.17}$$

and we set $V_\infty = V_0 \cup V_1 \cup V_2 \cup \cdots$. Clearly this is not a very explicit form for the mainstream solution, but it does converge and could be manipulated numerically.

We have completed our asymptotic description of the solution in the mainstream and in the boundary layers. We now need to satisfy the integral constraint (6.3), i.e., $\Delta = 1$. To do this we first fix a parameter μ with $\sqrt{\varepsilon} \ll \mu \ll 1$. In the boundary layer we use the leading order approximation $\lambda \simeq \beta$ and $q_{\rm R} \simeq 1/2$. We can then solve the integral equation (6.6)

numerically for these values, and the solution depicted in figure 20 confirms the scaling behaviours in (6.7) and (6.8) above. We now extract from (6.8) that

$$\int_{1-\mu}^{1} b'(x)\,dx = \int_{-\mu\varepsilon^{-1/2}}^{0} d'(X)\,dX = C_{\rm R} + f_{\rm R}\log(\mu\varepsilon^{-1/2}), \tag{6.18}$$

where the constants $C_{\rm R} < 0$ and $f_{\rm R} < 0$ can be obtained numerically, and depend on the value of α, but not on ε.

Now in the mainstream region we set

$$q_{\rm R} = 1/2 + \delta q, \quad \lambda = \beta + \delta\lambda, \quad \delta\lambda \simeq (-2\beta\log\beta)\delta q, \quad \delta q, \delta\lambda = o(\varepsilon), \tag{6.19}$$

and retain leading effects in δq, $\delta\lambda$. We may evaluate

$$\int_{-1}^{1-\mu} b'(x)\,dx = f_{\rm R}(-2\delta q)^{-1}[(2\varepsilon^{-1/2})^{-2\delta q} - (\mu\varepsilon^{-1/2})^{-2\delta q}] + I_{\rm conv}, \tag{6.20}$$

using (6.9), (6.11) and (6.15). Here $I_{\rm conv}$ is the contribution from $b'_{\rm conv}$. Let us drop this term to simplify the ensuing argument, and revisit this later.

Summing (6.18) and (6.20) and approximating the terms in μ, then yields

$$\Delta = C_{\rm R} + f_{\rm R}(-2\delta q)^{-1}[(2\varepsilon^{-1/2})^{-2\delta q} - 1], \tag{6.21}$$

and putting $\Delta = 1$ gives the equation

$$-C \equiv f_{\rm R}^{-1}(1 - C_{\rm R}) = (-2\delta q)^{-1}[(2\varepsilon^{-1/2})^{-2\delta q} - 1] \tag{6.22}$$

for δq. Now in the boundary layer we will have $C_{\rm R} < 0$, $f_{\rm R} < 0$, giving $C > 0$, so that the left-hand side is negative, whereas for any real, non-zero δq, the right-hand side is positive. Thus δq must be complex, as argued originally.

We can rewrite (6.22) as

$$1 + 2C\delta q = (2\varepsilon^{-1/2})^{-2\delta q} \equiv e^{-2\delta q\log(2\varepsilon^{-1/2})}. \tag{6.23}$$

The argument of the left-hand side is approximately $2C\delta q_{\rm i} - 2n\pi$ where subscripts 'r' and 'i' denote real and imaginary parts and n is any integer. Equating arguments of both sides of the equation gives at leading order

$$\delta q_{\rm i} = n\pi/\log(2\varepsilon^{-1/2}) \qquad (n \neq 0). \tag{6.24}$$

Curiously this does not require knowledge of C, so in fact there is no need to solve the boundary layer problem numerically!

Looking at the modulus of (6.23) would yield

$$\delta q_{\rm r} = -C^2 n^2\pi^2[\log(2\varepsilon^{-1/2})]^{-3}. \tag{6.25}$$

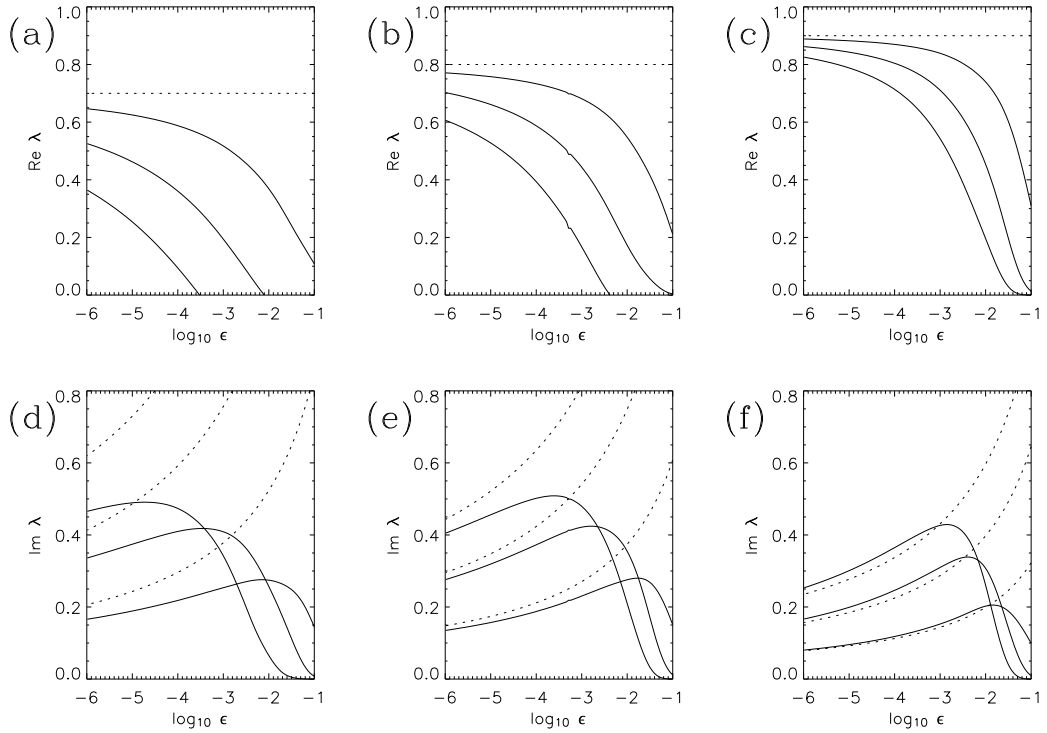

Fig. 21. Plot of eigenvalues λ against $\log_{10}\varepsilon$ with numerical results shown solid and the leading approximation (6.26) dotted, for the leading three branches. In (a–c) $\mathrm{Re}\,\lambda$ is plotted and in (d–f) $\mathrm{Im}\,\lambda$ is shown for (a,d) $\alpha = 0.3$, (b,e) $\alpha = 0.2$ and (c,f) $\alpha = 0.1$.

This is quite a small term, given that our expansion is in powers of $(\log\varepsilon^{-1})^{-1}$. In fact numerical study of δq_{r} reveals that it scales as $(\log\varepsilon^{-1})^{-2}$. We therefore conclude that the approximation (6.25) is giving a subdominant effect, and we can only say that $\delta q_{\mathrm{r}} = 0$ to the order at which we are working.

We finally obtain the eigenvalue, correct up to order $(\log\varepsilon^{-1})^{-1}$ as

$$\lambda = \beta - \frac{2in\pi\beta\log\beta}{\log(2\varepsilon^{-1/2})} \qquad (n \neq 0), \tag{6.26}$$

valid for $\alpha < \beta$. To check this is correct, figure 21 shows real and imaginary parts of the eigenvalues (solid) compared with the leading approximation (dotted) for the leading three branches, $n = 1, 2, 3$. Given that the approximation goes in inverse powers of $\log\varepsilon^{-1}$, the agreement is good, especially as α is reduced. It is probable that this is because the left-hand boundary layer, negligible for any fixed $\alpha < 1/2$ in the limit $\varepsilon \to 0$, will tend to reassert itself for fixed ε and α increasing towards $1/2$.

Finally we discuss briefly the contribution from I_{conv} to the problem, which we dropped above. For $\delta q = 0$ the contribution from I_{conv} is real and negative, and so this component can be bundled in with C in (6.22) without changing

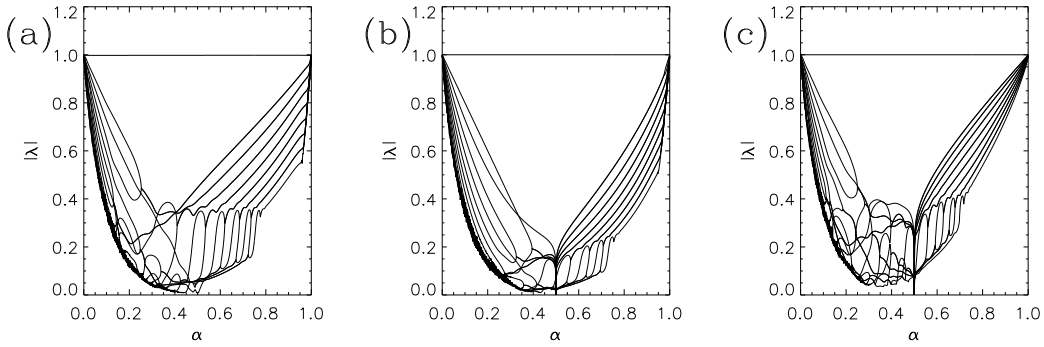

Fig. 22. Moduli of eigenvalues $|\lambda|$ as a function of α for (a) zero (Z), (b) no-flux (F), and (c) periodic (P) boundary conditions, with $\varepsilon = 10^{-5}$, $N = 1024$.

the result (6.24). Now as δq increases and becomes complex, so will $I_{\rm conv}$; however it can be shown that $I_{\rm conv}(\delta q) = I_{\rm conv}(0) + O(\delta q)$ (using the geometrical convergence present in (6.16)) and so the variation of $I_{\rm conv}$ with δq would be a subdominant effect if put into (6.23); the dominant effect would still come from the right-hand side. In conclusion, our result (6.26) remains valid for small ε.

7 Numerical results and theory for the stretch–fold map

This map is defined by

$$Ta(x) = \begin{cases} a(\alpha^{-1}(x+\beta)) & (-1 \le x \le \Upsilon), \\ a(\beta^{-1}(\alpha - x)) & (\Upsilon < x \le 1), \end{cases} \tag{7.1}$$

and corresponds to figure 1, except that the second piece is rotated by π radians before being reassembled. This map is a simple model of folding in a fluid flow, and forms the basis of the stretch–fold–shear dynamo model [7]. We consider it briefly here, as it has some features that distinguish it from the stretch–stack model defined back in (2.3). The corresponding adjoint operator is

$$T^*b(x) = \alpha b(\alpha x - \beta) + \beta b(\alpha - \beta x). \tag{7.2}$$

Eigenvalues for $\varepsilon = 10^{-5}$ and the three key boundary conditions are shown in figure 22. For $\alpha = \beta = \frac{1}{2}$ super-exponential decay occurs for all fields with the (F) boundary condition, and with (P) for the subspace of non-constant, even fields ($n > 0$ and even in (A.3)).

In the absence of diffusion, we can define operators $\mathcal{T}^*$ (as in (7.2)), with

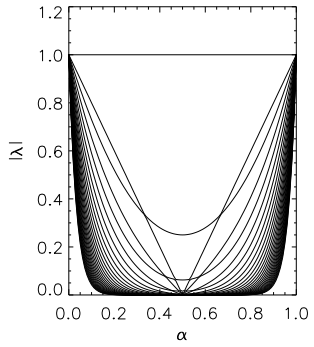

Fig. 23. Moduli of eigenvalues, $|\lambda_{(n)}|$ of $\mathcal{T}$ or $\mathcal{T}^*$ as a function of α for the stretch–fold map.

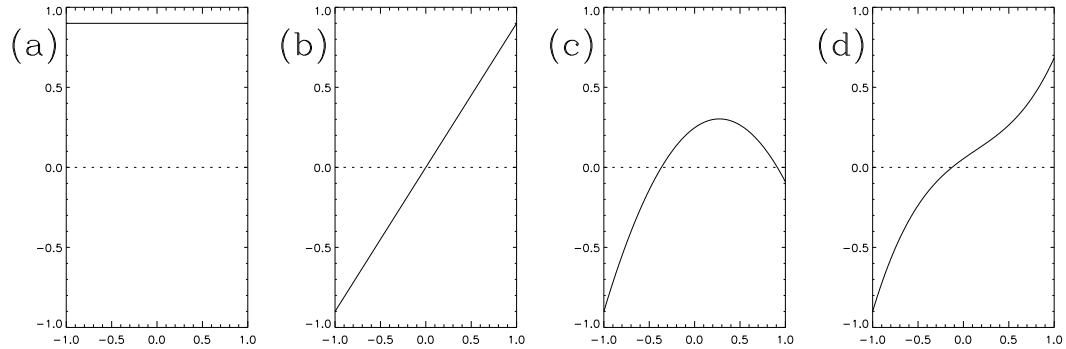

Fig. 24. Leading four adjoint eigenfunctions $b_{(n)}$ for $\alpha = 0.3$ and zero diffusion; in (a,b,c,d) $n = 0, 1, 2, 3$.

matrix elements

$$\mathcal{T}^*_{mn} = \frac{n!}{m!(n-m)!} r^{m-n} (\alpha^{m+1}(-\beta)^{n-m} - (-\beta)^{m+1}\alpha^{n-m}) \qquad (7.3)$$

(for $m \le n$) and $\mathcal{T}$ given by

$$\mathcal{T}a(z) = a(\alpha^{-1}(z+\beta)) - a(\beta^{-1}(\alpha - z)). \qquad (7.4)$$

These have eigenvalues shown in figure 23,

$$\lambda_{(n)} = \alpha^{n+1} - (-\beta)^{n+1} \qquad (n \ge 0). \qquad (7.5)$$

The leading mode remains (2.7), and the next eigenfunctions of $\mathcal{T}^*$ are given by

$$b_{(1)} = x, \quad b_{(2)} = x^2 + 2\,\frac{\Upsilon + 1}{3\Upsilon - 1}\,x - \tfrac{1}{3}, \qquad (7.6)$$

(except for $\alpha = 2/3$, $\Upsilon = 1/3$, when there is a degeneracy $\lambda_{(1)} = \lambda_{(2)}$). The corresponding eigenfunctions of $\mathcal{T}$ again take the form of distributions and can be defined as in (4.26), but the weights are now defined recursively by

$$W_m = \{(\alpha y - \beta, \alpha^{n+1}\lambda_{(n)}^{-1} w), (\alpha - \beta y, -(-\beta)^{n+1}\lambda_{(n)}^{-1} w) : (y, w) \in W_{m-1}\}. \qquad (7.7)$$

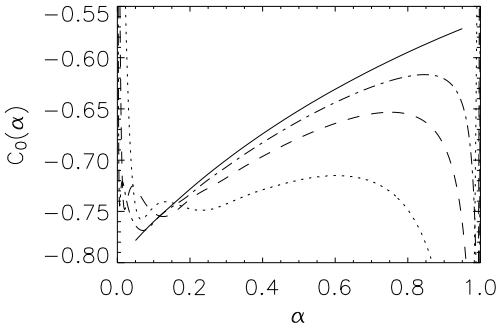

Fig. 25. Comparison of boundary layer calculation. $C_0(\alpha)$ is plotted against α for $0.06 \leq \alpha \leq 0.94$ (solid). Also $\varepsilon^{-1/2}(\lambda - 1)$ is plotted for $\varepsilon = 10^{-3}$ (dot), 10^{-4} (dash) and 10^{-5} (dot–dash) with the (Z) boundary condition.

Note that for eigenfunctions with n odd the weights now vary in sign; for example for $n = 1$ this arises because of the reversal of scalar gradients by the folding action of the mapping (7.1). The definition is then reminiscent of a sign-singular measure [12]. With this framework we can again address the effects of diffusion using perturbation theory.

7.1 Decay with the zero boundary condition

For the zero boundary condition the theory is very similar to that in section 3. The main difference is that whereas applying H_ε generates both a left- and a right-hand boundary layer, the action of T^* is to fold these two boundary layers over to the left-hand side. Thus in our perturbative approach we have the source term

$$T_1^* b_0(-1 + \sqrt{\varepsilon}X) = -2\alpha g_0(\alpha X) - 2\beta g_0(\beta X) \tag{7.8}$$

in place of (3.11) and there is no right-hand boundary layer to consider. The theory goes through as before to give $\lambda_1 = \lambda_{1\mathrm{L}} = C_0(\alpha)\sqrt{\varepsilon}$ with $C_0(\alpha)$ shown in figure 25; there is good agreement with numerical results.

7.2 Decay with the no-flux boundary condition

More interesting is the case of the no-flux boundary condition. Again there is just one, left-hand boundary layer to be considered. The conditions for robustness then become

$$|\lambda_0| > \alpha \qquad \text{(Z) or (P)}, \tag{7.9}$$
$$|\lambda_0| > \alpha^2 \qquad \text{(F)}, \tag{7.10}$$

in general accord with the numerical results shown in figure 22.

For the (F) boundary condition, the decay of scalar fluctuations is dominated by the $\lambda_{(1)} = \alpha^2 - \beta^2$ branch for $\alpha < 1/3$ and by the $\lambda_{(2)} = \alpha^3 + \beta^3$ branch for $1/3 < \alpha < 1/2$. For $\alpha > 1/2$ it is dominated by diffusive modes.

We consider here only the range $0 < \alpha < 1/3$ for which $\lambda_{(1)}$ is dominant; $\lambda_{(1)}$ is also negative in this range, which makes the exponent q below complex. The boundary layer calculations proceed as before for the left-hand boundary layer with the source term

$$T_1'^* b_0'(-1 + \sqrt{\varepsilon}X) \simeq -2\alpha^2 g_0(\alpha X) + 2\beta^2 g_0(\beta X), \tag{7.11}$$

where

$$T'^* b'(x) = \alpha^2 b'(\alpha x - \beta) - \beta^2 b'(\alpha - \beta x). \tag{7.12}$$

In the far field q becomes complex in the equation analogous to (5.14) and we can write

$$2q = 2\tilde{q} + i\pi/\log\alpha, \qquad 2\tilde{q}(\alpha) \equiv 2 - \frac{\log|\lambda_0|}{\log\alpha}, \tag{7.13}$$

so that, for the stretch–fold model, we have

$$d'(X) = X^{-2\tilde{q}}\tilde{f}(\log X), \qquad \tilde{f}(\log X + \log\alpha) = -\tilde{f}(\log X). \tag{7.14}$$

$\tilde{f}$ now varies in sign and has period $2\log\alpha$ in $\log X$. The boundary layer has an oscillatory tail, as it is trying to match to an eigenfunction in the mainstream with a negative eigenvalue.

The calculations now proceed to yield the correction as

$$\lambda_1 = \lambda_{1\mathrm{L}} = C_1(\alpha, \varepsilon)\varepsilon^{\tilde{q}(\alpha)}, \tag{7.15}$$

with

$$C_1(\alpha, \varepsilon) = \lambda_0 \lim_{m\to\infty} \sum_{(y,w)\in W_m, y>\Upsilon} w\,(y+1)^{-2\tilde{q}}\tilde{f}(\log(y+1) - \tfrac{1}{2}\log\varepsilon) \tag{7.16}$$

in place of (5.23). We see that for the stretch–fold model the correction λ_1 is a power law with oscillations in sign of period $2\log\alpha$ in the variable $\frac{1}{2}\log\varepsilon$, for $\alpha < 1/3$. (For $1/3 < \alpha < 1/2$ there are no oscillations.) A similar non-monotonic approach of λ to λ_0 as $\varepsilon \to 0$ is seen in a closely related model [13] (also involving a fold in the mapping).

To test this theory figure 26 shows a comparison of numerical results (solid) with theory (dashed) for (a) $\alpha = 0.3$ and (b) $\alpha = 0.1$. In each case the correction $|\lambda_1|$ is plotted against ε in a log–log scale. Clearly visible are oscillations in the numerical results and as $\varepsilon \to 0$ there is excellent agreement with the theoretical results, which were obtained by solving the boundary layer equation analogous to (5.12) (but with the source term (7.11)) and then computing

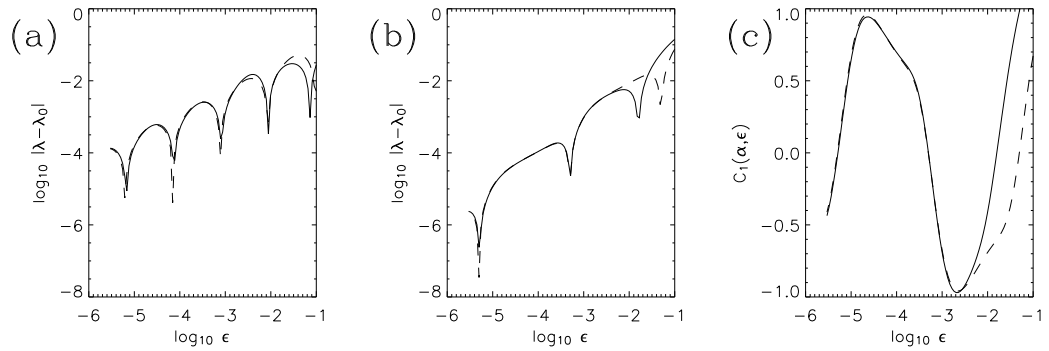

Fig. 26. Comparison of boundary layer theory and numerical simulations for the (F) boundary condition. For (a) $\alpha = 0.3$ and (b) $\alpha = 0.1$, plotted is $\log_{10}|\lambda - \lambda_0|$ against $\log_{10}\varepsilon$ (solid), with the asymptotic approximation (7.15) (dashed). In (c), for $\alpha = 0.1$ the quantities $\varepsilon^{-\tilde{q}}(\lambda - \lambda_0)$ (solid) and $C_1(\alpha, \varepsilon)$ (dashed) are plotted against $\log_{10}\varepsilon$.

$C_1(\alpha, \varepsilon)$ from (7.16) for each value of ε. Note that the phase and sign of the oscillations are predicted correctly, and that the oscillations are not purely sinusoidal as seen in figure 26(c), showing $C_1(\alpha, \varepsilon)$ for $\alpha = 0.1$.

8 Discussion

We have discussed the decay of passive scalars in baker's maps with uneven stretching, under the influence of weak diffusion. We have found rather a complicated set of results, which we have set out already in section 2. Some of the surprises involve the sensitivity to boundary conditions: for example the decay of scalar fluctuations is quite different in the cases of no-flux and periodic boundary conditions.

We have also seen significant differences in behaviour between a baker's map where the two pieces are stacked together (see figure 1), and where one piece is rotated to give a fold in the scalar in section 7. These maps have identical stretching properties, but different properties in terms of reversals of scalar gradients. One possible direction of research would be to try to quantify the differences between the two mappings in terms of a cancellation exponent [12]; the different forms of the direct eigenfunctions (see (4.25) and (7.7)) are suggestive of a link, as the stretch–fold (strange) eigenfunction has oscillations in sign on arbitrarily small scales. It would also be interesting to link the strange eigenfunctions we have constructed to the study [1] giving the initial decay of scalar fields in terms of the distribution of finite time Lyapunov exponents, and more generally to the fractal properties of the scalar field [25].

During our study we set down a problem of scalar advection without diffusion, by defining the operators $\mathcal{T}$ and $\mathcal{T}^*$. The eigenvalues $\lambda_{(n)}$ so obtained gave us

a problem to which we could apply perturbation theory. The eigenvalues are in fact the same as Ruelle–Pollicott resonances [29,32] as shown in [33], which give the decay of correlations in the system, i.e., the decay of quantities such as

$$(b, T^n a) \equiv (T^{*n} b, a) \tag{8.1}$$

in the limit of large n, where b and a are smooth functions.

In these terms, we have been investigating when the effect of diffusion on a scalar field is equivalent to the decay of correlations in the scalar field under iteration of T. To summarise our results, we have found that the effect of boundary conditions and the magnitude of the decay rate $|\lambda|$ are crucial. The larger $|\lambda|$ is, and the weaker the boundary layers developed, the more likely is the decay of a passive scalar to be governed by the Ruelle–Pollicott resonance. The precise results are given in (5.1)–(5.3). The analogous question in the fast dynamo problem is when the growth of magnetic fluxes for zero diffusion corresponds to the growth of magnetic fields for very weak diffusion; this has been referred to as the 'flux conjecture' and there is much evidence that it is correct, at least for the case of growing magnetic fields [10,18].

In terms of extending our study, it would be good to have a rigorous proof that gives the citeria (5.1)–(5.3) for the perfect modes to be robust to diffusion. It would also be of interest to consider two-dimensional hyperbolic maps, with both a contracting and an expanding direction and understand the links between the Ruelle–Pollicott resonances and the decay of passive scalars in this case. Real fluid flows, of course, tend to lack such uniformly hyperbolic behaviour and the decay of passive scalars tends to be dominated by islands if they are present. This is a subject of active research, both on the relation between Ruelle–Pollicott resonances and the decay of correlations [17,22,36], and how these link to passive scalar decay rates [28].

A Appendix: matrix elements in L^2

In this appendix we give the orthonormal bases and matrix elements used for numerical computations of eigenvalues and eigenvectors in section 2 above. The basis for the zero (Z) boundary condition is indexed by $n \geq 1$:

$$\psi_n(x) = \sin \tfrac{1}{2} n\pi(x+1) \qquad (n \geq 1) \qquad \text{(Z)}. \tag{A.1}$$

For the no-flux (F) boundary condition we use, indexed by $n \geq 0$,

$$\psi_n(x) = \cos \tfrac{1}{2} n\pi(x+1) \quad (n \geq 1), \quad \psi_0(x) = 2^{-1/2} \qquad \text{(F)}, \tag{A.2}$$

and for the periodic (P) boundary condition we use, indexed by $n \geq 0$,

$$\psi_n(x) = \begin{cases} 2^{-1/2} & (n=0), \\ \cos q\pi x & (n \text{ even}, n = 2q > 0), \\ \sin q\pi x & (n \text{ odd}, n = 2q-1). \end{cases} \qquad \text{(P)}, \tag{A.3}$$

It is convenient to define $F(k) = 2k^{-1}\sin k$ and coefficients ν_m by

$$\nu_0 = 2^{-1/2}, \quad \nu_m = 1 \quad (m > 0). \tag{A.4}$$

The matrix elements for (Z) (upper sign) and (F) (lower sign) with the appropriate ranges of m and n are,

$$\begin{aligned} T_{mn} = \tfrac{1}{2}\alpha\nu_m\nu_n[&\pm \cos\tfrac{1}{2}\pi(m\alpha+n)\, F(\tfrac{1}{2}\pi(m\alpha+n)) \\ &+ \cos\tfrac{1}{2}\pi(m\alpha-n)\, F(\tfrac{1}{2}\pi(m\alpha-n))] \\ +\tfrac{1}{2}\beta\nu_m\nu_n[&\pm \cos\tfrac{1}{2}\pi(m(\beta-2)-n)\, F(\tfrac{1}{2}\pi(m\beta+n)) \\ &+ \cos\tfrac{1}{2}\pi(m(\beta-2)+n)\, F(\tfrac{1}{2}\pi(m\beta-n))]. \end{aligned} \tag{A.5}$$

For the heat kernel H_ε we have for either basis

$$H_{\varepsilon mn} = e^{-\varepsilon n^2\pi^2/4}\delta_{mn}. \tag{A.6}$$

The zero–no-flux (ZF) boundary condition is given simply by restricting m and n to odd values and replacing $\frac{1}{2}\pi$ by $\frac{1}{4}\pi$ in (A.1), in (A.5) with the lower signs, and in (A.6).

For the (P) boundary condition,

$$\begin{aligned} T_{mn} = \tfrac{1}{4}\nu_m\nu_n\, &i^{\frac{1}{2}(\rho-1)}\, i^{\frac{1}{2}(\sigma-1)} \\ &\times[\alpha(\rho\sigma e^{i\pi p\beta} + e^{-i\pi p\beta})(F(\pi(p\alpha+q)) + \sigma F(\pi(p\alpha-q))) \\ &+\beta(e^{i\pi p\alpha} + \rho\sigma e^{-i\pi p\alpha})(F(\pi(p\beta+q)) + \sigma F(\pi(p\beta-q)))], \end{aligned} \tag{A.7}$$

where we let $(p,\rho) = (m/2, 1)$ if m is even, and $(\frac{1}{2}(m+1), -1)$ if m is odd. We define (q,σ) similarly in terms of n. In this case we have also for the heat kernel

$$H_{\varepsilon mn} = e^{-\varepsilon p^2\pi^2}\delta_{mn}. \tag{A.8}$$

For the stretch–fold model (7.1), the final terms in equations (A.5) and (A.7) are replaced by, respectively,

$$\begin{aligned} \cdots + \tfrac{1}{2}\beta\nu_m\nu_n[&\cos\tfrac{1}{2}\pi(m(\beta-2)+n)\, F(\tfrac{1}{2}\pi(m\beta+n)) \\ &\pm \cos\tfrac{1}{2}\pi(m(\beta-2)-n)\, F(\tfrac{1}{2}\pi(m\beta-n))], \end{aligned} \tag{A.9}$$

$$\cdots + \beta(e^{i\pi p\alpha} + \rho\sigma e^{-i\pi p\alpha})(\sigma F(\pi(p\beta+q)) + F(\pi(p\beta-q)))]. \tag{A.10}$$

B Appendix: spectra of T and T^* in L^2

In this section we discuss briefly the spectra of the diffusionless baker's map operators T and T^* in L^2; a more extended discussion for the dynamo problem may be found in [18]. We use the framework in [9,10]; related results for Anosov diffeomorphisms may be found in [3,11,24].

The spectrum $\sigma(A)$ of an operator A, in L^2 say, is the set of $\lambda \in \mathbb{C}$ for which $\lambda I - A$ is not invertible as a bounded operator in L^2. For λ in the point spectrum $\sigma_{\rm p}(A)$, there are eigenvectors of A, $Av = \lambda v$; for λ in the approximate spectrum $\sigma_{\rm ap}(A)$, $\lambda I - A$ is not bounded below, and for λ in the compression spectrum $\sigma_{\rm com}(A)$, the image of $\lambda I - A$ is not dense in L^2.

We use the general results for an operator A and its adjoint A^*,

$$\sigma(A) = \sigma(A^*) \text{ is a closed subset of } \{\lambda : |\lambda| \le \|A\|\}, \tag{B.1}$$
$$\sigma(A) = \sigma_{\rm ap}(A) \cup \sigma_{\rm com}(A), \tag{B.2}$$
$$\sigma_{\rm p}(A) \subset \sigma_{\rm ap}(A), \tag{B.3}$$
$$\sigma_{\rm com}(A) = \sigma_{\rm p}(A^*), \tag{B.4}$$
$$\partial\sigma(A) \subset \sigma_{\rm ap}(A), \tag{B.5}$$

and the following specific properties of T and T^*

$$T \text{ is an isometry, } \|Ta\| = \|a\|, \tag{B.6}$$
$$T^*T = I. \tag{B.7}$$

Equation (B.6) implies that $\|T\| \equiv \|T^*\| = 1$.

First we show that any λ with $|\lambda| < 1$ is an eigenvalue of T^* and so in $\sigma_{\rm p}(T^*)$. To do so choose such a λ and a function $f(x)$ in the kernel of T^*, for example

$$f(x) = \begin{cases} \alpha^{-1} \sin \pi(x+1)/2\alpha & (-1 \le x \le \Upsilon), \\ \beta^{-1} \sin \pi(x-1)/2\beta & (\Upsilon < x \le 1), \end{cases} \tag{B.8}$$

then the function defined by the sum (convergent in L^2)

$$b = \sum_{n=0}^{\infty} \lambda^n T^n f \tag{B.9}$$

satisfies $T^*b = \lambda b$ by virtue of (B.7). Note however that eigenfunctions constructed in this manner generally have structure on all scales, and fail to be infinitely differentiable, no matter how smooth we make f [18]. They are thus not generally robust to the effects of diffusion.

At the end of this appendix we will show that the only eigenvalue λ of T or of T^* with $|\lambda| = 1$ is given by the constant scalar mode (2.7). Also from (B.6)

all eigenvalues of T must have modulus $|\lambda| = 1$, and so

$$\sigma_{\rm p}(T) = \sigma_{\rm com}(T^*) = \{1\}, \qquad \sigma_{\rm p}(T^*) = \sigma_{\rm com}(T) = \{1\} \cup \mathrm{Int}\,\Delta, \tag{B.10}$$

where $\Delta \equiv \{\lambda : |\lambda| \le 1\}$ and Int denotes its interior. Given that $\|T\| = 1$ (B.1) implies that

$$\sigma(T) = \sigma(T^*) = \Delta. \tag{B.11}$$

Now (B.6) also implies that any $\lambda \in \sigma_{\rm ap}(T)$ has modulus $|\lambda| = 1$ and so, with (B.3) and (B.5), we have

$$\sigma_{\rm ap}(T) = \partial\Delta, \qquad \sigma_{\rm ap}(T^*) = \Delta. \tag{B.12}$$

Finally we may define residual spectrum $\sigma_{\rm r}$ and continuous spectrum $\sigma_{\rm com}$ of an operator A by

$$\sigma_{\rm r}(A) = \sigma_{\rm com}(A) \setminus \sigma_{\rm p}(A), \qquad \sigma_{\rm c}(A) = \sigma(A) \setminus \{\sigma_{\rm com}(A) \cup \sigma_{\rm p}(A)\}, \tag{B.13}$$

to give

$$\sigma_{\rm r}(T) = \mathrm{Int}\,\Delta, \quad \sigma_{\rm r}(T^*) = \emptyset, \quad \sigma_{\rm c}(T) = \sigma_{\rm c}(T^*) = \partial\Delta \setminus \{1\}. \tag{B.14}$$

With $\sigma(A) = \sigma_{\rm p}(A) \cup \sigma_{\rm c}(A) \cup \sigma_{\rm r}(A)$ as a disjoint union, the results in (B.10) and (B.14) are summarised in figure 12(c,d).

To conclude we show that the only eigenvalue λ of T or T^* with $|\lambda| = 1$ is $\lambda = 1$, corresponding to the constant scalar mode (2.7). To do so we first note that an eigenfunction b of T eigenvalue λ immediately gives one of T^* eigenvalue λ^{-1}. That is, $Ta = \lambda a$ implies $T^*a = \lambda^{-1}a$, from (B.7). It therefore suffices to consider T and, to exclude the constant scalar mode, consider only scalar fields a with zero mean.

We define a basis for zero-mean fields in L^2 by first setting

$$\psi(x) = \begin{cases} -(\beta/2\alpha)^{1/2} & (-1 \le x \le \Upsilon), \\ (\alpha/2\beta)^{1/2} & (\Upsilon < x \le 1). \end{cases} \tag{B.15}$$

We obtain two *descendants* $\psi_0 = S_0\psi$, $\psi_1 = S_1\psi$ of ψ with

$$S_0\psi(x) = \begin{cases} \alpha^{-1/2}\psi(\alpha^{-1}(x+\beta)) & (-1 \le x \le \Upsilon), \\ 0 & (\Upsilon < x \le 1), \end{cases} \tag{B.16}$$

$$S_1\psi(x) = \begin{cases} 0 & (-1 \le x \le \Upsilon), \\ \beta^{-1/2}\psi(\beta^{-1}(x-\alpha)) & (\Upsilon < x \le 1). \end{cases} \tag{B.17}$$

Applying S_0 and S_1 repeatedly to ψ gives an orthonormal basis (essentially a Haar basis) $\{\psi_s\}$ of L^2, labelled by finite binary strings s. Here $S_0\psi_s = \psi_{s0}$

and $S_1\psi_s = \psi_{s1}$ are the descendants of ψ_s. The operator T maps members of this basis onto their descendants only

$$T\psi_s = \alpha^{1/2}\psi_{s0} + \beta^{1/2}\psi_{s1}. \tag{B.18}$$

If a zero-mean scalar field a is expanded in this basis, then from $Ta = \lambda a$ it may be seen that all the expansion coefficients are zero, and so there are no eigenfunctions of T for any λ, except for (2.7).

Acknowledgements

I am grateful to Erik Aurell, Steve Childress, Anton Deitmar, Erwan Hascoët, Ben Mestel and Jean-Luc Thiffeault for valuable discussions and references.

This study was begun at the 'Geometry and Topology of Fluid Flows' programme held at the Isaac Newton Institute in Cambridge (Autumn 2000) and completed at the programme 'Magnetohyodrodynamics of Stellar Interiors' (Autumn 2004). I an grateful to the organisers and directors for inviting me to participate.

References

[1] Antonsen, T.M., Fan, Z., Ott, E. & Garcia–Lopez, E. 1996 The role of chaotic orbits in the determination of power spectra of passive scalars. *Phys. Fluids* **8**, 3094–3104.

[2] Aref, H. 1983 Stirring by chaotic advection. *J. Fluid Mech.* **143**, 1–21.

[3] Arnold, V.I. & Avez, A. 1967 *Problèmes Ergodiques de la Mécanique Classique*. Gauthier–Villars, Paris. [English transl.: *Ergodic Problems of Classical Mechanics*. Benjamin (1968).]

[4] Aurell, E. & Gilbert, A.D. 1993 Fast dynamos and determinants of singular integral operators. *Geophys. Astrophys. Fluid Dyn.* **73**, 5–32.

[5] Balmforth, N.J., Cvitanović, P., Ierley, G.R., Spiegel, E.A. & Vattay, G. 1993 Advection of vector fields by chaotic flows. In *Stochastic Processes in Astrophysics*, pp. 148–160. Annals New York Acad. Sci., vol. 706.

[6] Bayly, B.J. 1994 Maps and dynamos. In *Lectures on Solar and planetary dynamos* (ed. M.R.E. Proctor, A.D. Gilbert), pp. 305–329. Cambridge University Press.

[7] Bayly, B.J. & Childress, S. 1988 Construction of fast dynamos using unsteady flows and maps in three dimensions. *Geophys. Astrophys. Fluid Dyn.* **44**, 211–240.

[8] Bayly, B.J. & Childress, S. 1989 Unsteady dynamo effects at large magnetic Reynolds numbers. *Geophys. Astrophys. Fluid Dyn.* **49**, 23–43.

[9] Bollobás, B. 1990 *Linear Analysis: An Introductory Course.* Cambridge University Press.

[10] Childress, S. & Gilbert, A.D. 1995 *Stretch, Twist, Fold: The Fast Dynamo.* Springer–Verlag.

[11] de la Llave, R. 1993 Hyperbolic dynamical systems and generation of magnetic fields by perfectly conducting fluids. *Geophys. Astrophys. Fluid Dyn.* **73**, 123–131.

[12] Du, Y., Tél, T. & Ott, E. 1994 Characterization of sign singular measures. *Physica D* **76**, 168–180.

[13] Eckhardt, B., Hascoët, E. & Braun, W. 2003 Passive fields and particles in chaotic flows. In *Proc. IUTAM Symposium on Nonlinear Stochastic Dynamics* (ed. N Sri Namachchivaya, Y.K. Lin), book series *Solid Mechanics and its Applications*, vol. 110. Kluwer.

[14] Fereday, D.R., Haynes, P.H., Wonhas, A. & Vassilicos, J.C. 2002 Scalar variance decay in chaotic advection and Batchelor-regime turbulence. *Phys. Rev. E* **65**, article 035301.

[15] Finn, J.M. & Ott, E. 1988 Chaotic flows and fast magnetic dynamos. *Phys. Fluids* **31**, 2992–3011.

[16] Finn, J.M. & Ott, E. 1990 The fast kinematic magnetic dynamo and the dissipationless limit. *Phys. Fluids B* **2**, 916–926.

[17] Fishman, S. & Rahav, S. 2002 Relaxation and noise in chaotic systems. In *Dynamics of Dissipation* (ed. P. Garbaczewski, R. Olkiewicz), Lecture Notes in Physics, vol. 597, pp. 165–192. Springer-Verlag.

[18] Gilbert, A.D. 2002 Advected fields in maps: I. Magnetic flux growth in the stretch–fold–shear map. *Physica D* **166**, 167–196.

[19] Gilbert, A.D. 2004 Advected fields in maps: II. Dynamo action in the stretch–fold–shear map. *Geophys. Astrophys. Fluid Dyn.*, submitted.

[20] Hasegawa, H.H. & Saphir, W.C. 1992 Unitarity and irreversibility in chaotic systems. *Phys. Rev. A* **46**, 7401–7423.

[21] Kato, T. 1980 *Perturbation Theory for Linear Operators.* Springer–Verlag.

[22] Khodas, M., Fishman, S. & Agam, O. 2000 Relaxation to the invariant density for the kicked rotor. *Phys. Rev. E* **62**, 4769–4783.

[23] Liu, W. & Haller, G. Strange eigenmodes and decay of variance in the mixing of diffusive tracers. *Physica D* **188**, 1–39.

[24] Mather, J.N. 1968 Characterization of Anosov diffeomorphisms. *Indagat. Math.* **30**, 479–483.

[25] Ott, E. & Antonsen, T.M. 1989 Fractal measures of passively convected vector fields and scalar gradients in chaotic fluid flows. *Phys. Rev. A* **39**, 3660–3671.

[26] Ottino, J.M. 1989 *The kinematics of mixing: stretching, chaos and transport.* Cambridge University Press.

[27] Pierrehumbert, R.T. 1994 Tracer microstructure in the large-eddy dominated regime. *Chaos, Solitons & Fractals* **4**, 1091–1110.

[28] Pikovsky, A. & Popovych, O. 2003 Persistent patterns in deterministic mixing flows. *Europhys. Lett.* **61**, 625–631.

[29] Pollicott, M. 2002 Periodic orbits and zeta functions. In *Handbook of dynamical systems*, vol. 1A (ed. B. Hasselblatt, A. Katok), Elsevier Science B.V.

[30] Rado, A. 1993 *Onset and Intermittency in the SFS Map.* MS Thesis, Courant Institute of Mathematical Sciences, New York University.

[31] Rothstein, D., Henry, E. & Gollub, J.P. 1999 Persistent patterns in transient chaotic fluid mixing. *Nature* **401**, 770–772.

[32] Ruelle, D. 1986 Resonances of chaotic dynamical systems. *Phys. Rev. Lett.* **56**, 405–407.

[33] Rugh, H.H. 1992 The correlation spectrum for hyperbolic analytic maps. *Nonlinearity* **5**, 1237–1263.

[34] Thiffeault, J.-L. 2004 The strange eigenmode in Lagrangian coordinates. *Chaos* **14**, 531–538.

[35] Schlichtkrull, H. 1984 *Hyperfunctions and Harmonic Analysis on Symmetric Spaces.* Birkhäuser.

[36] Weber, J., Haake, F. & Seba, P. 2000 Frobenius–Perron resonances for maps with a mixed phase space. *Phys. Rev. Lett.* **85**, 3620–3623.

[37] Wonhas, A. & Vassilicos, J.C. 2002 Mixing in fully chaotic flows. *Phys. Rev. E.* **66**, article 051205.